Please cite this article in press as: Aguilo et al., THAP1: Role in Mouse Embryonic Stem Cell Survival and Differentiation, Stem Cell Reports (2017), http://dx.doi.org/10.1016/j.stemcr.2017.04.032

Stem Cell Reports
Article

ISSCR

OPEN ACCESS

THAP1: Role in Mouse Embryonic Stem Cell Survival and Differentiation

Francesca Aguilo,[1,2,10,*] Zuchra Zakirova,[3] Katie Nolan,[3] Ryan Wagner,[4,5] Rajal Sharma,[1] Megan Hogan,[4,5] Chengguo Wei,[6] Yifei Sun,[1,2] Martin J. Walsh,[1,7] Kevin Kelley,[4] Weijia Zhang,[6] Laurie J. Ozelius,[8] Pedro Gonzalez-Alegre,[9] Thomas P. Zwaka,[4,5] and Michelle E. Ehrlich[2,3,7,*]

[1]Department of Pharmacological Sciences
[2]Department of Pediatrics
[3]Department of Neurology
[4]Department of Cell, Developmental and Regenerative Biology
[5]Black Family Stem Cell Institute
[6]Department of Medicine Bioinformatics Core
[7]Department of Genetics and Genomic Sciences
Icahn School of Medicine at Mount Sinai, New York, NY 10029, USA
[8]Department of Neurology, Harvard Medical School, Massachusetts General Hospital, Charlestown, MA 02129, USA
[9]Perelman Center for Cellular & Molecular Therapeutics, Department of Neurology, The Children's Hospital of Philadelphia, Perelman School of Medicine, University of Pennsylvania, Philadelphia, PA 19104, USA
[10]Present Address: Department of Medical Biosciences, Wallenberg Center for Molecular Medicine, Umeå University, 901 85 Umeå, Sweden
*Correspondence: francesca.aguilo@umu.se (F.A.), michelle.ehrlich@mssm.edu (M.E.E.)
http://dx.doi.org/10.1016/j.stemcr.2017.04.032

SUMMARY

THAP1 (THAP [Thanatos-associated protein] domain-containing, apoptosis-associated protein 1) is a ubiquitously expressed member of a family of transcription factors with highly conserved DNA-binding and protein-interacting regions. Mutations in *THAP1* cause dystonia, DYT6, a neurologic movement disorder. THAP1 downstream targets and the mechanism via which it causes dystonia are largely unknown. Here, we show that wild-type THAP1 regulates embryonic stem cell (ESC) potential, survival, and proliferation. Our findings identify THAP1 as an essential factor underlying mouse ESC survival and to some extent, differentiation, particularly neuroectodermal. Loss of THAP1 or replacement with a disease-causing mutation results in an enhanced rate of cell death, prolongs *Nanog*, *Prdm14*, and/or *Rex1* expression upon differentiation, and results in failure to upregulate ectodermal genes. ChIP-Seq reveals that these activities are likely due in part to indirect regulation of gene expression.

INTRODUCTION

THAP1 (THAP [Thanatos-associated protein] domain-containing, apoptosis-associated protein 1) is a member of a large family of proteins which are primarily transcription factors (Gervais et al., 2013; Roussigne et al., 2003). The THAP domain, an atypical zinc finger ($CysX_{2-4}CysX_{35-53}CysX_2His$), is highly conserved and is part of the DNA-binding domain (DBD) with homology to P-transposable elements (Majumdar and Rio, 2015). THAP1 mutations cause DYT6 dystonia (Fuchs et al., 2009), and mutations are located throughout the protein, with about 50% in the DNA-binding domain. Importantly, recessive mutations have been identified (Houlden et al., 2010; Schneider et al., 2011; Xiromerisiou et al., 2012). THAP1 functions, targets, and the mechanisms by which its mutations lead to dystonia are largely unknown, including the effects of mutations on DNA binding (Campagne et al., 2012).

Functional studies of THAP1 in human umbilical vein endothelial cells (HUVECs) show a role in the S phase of mitosis via modulation of pRb-E2F cell-cycle target genes, including *RRM1* (Clouaire et al., 2005). In vitro, a coiled-coil domain is required for dimerization (Sengel et al., 2011). Other interactors include prostate apoptosis response-4 protein (Par-4), an effector of cell death linked to prostate cancer and neurodegenerative diseases (Roussigne et al., 2003); HCF-1, a transcriptional co-activator involved in cell-cycle regulation; and O-GlcNAc transferase (OGT), which catalyzes the addition of O-GlcNAc and thereby also participates in epigenetic regulation of gene expression with an essential function in dividing cells (Mazars et al., 2010).

In mouse models of DYT6 which harbor either a disease-causing C54Y mutation in the DBD or a null allele (ΔExon2) (Ruiz et al., 2015), rare homozygous embryos survived to day 14. They were small with defects in peripheral organs and brain, which showed deficits in the number and morphology of neurons. To study the impact of the mutant alleles on stem cell maintenance and differentiation, we generated mouse embryonic stem cells (mESCs) homozygous for either the C54Y ($Thap1^{C54Y}$) or ΔExon2 ($Thap1^{\Delta Exon2}$) alleles. Herein, we characterize both ESCs, which are viable with intact stem cell characteristics, but with abnormalities in cell death, cell cycle, and proliferation rate, that are more severe in the ΔExon2 than in the C54Y homozygote. Furthermore, we show that during differentiation of embryoid bodies (EBs), wild-type THAP1 is required for repression of a cohort of core pluripotency-associated genes and survival in ΔExon2 cells, and

Please cite this article in press as: Aguilo et al., THAP1: Role in Mouse Embryonic Stem Cell Survival and Differentiation, Stem Cell Reports (2017), http://dx.doi.org/10.1016/j.stemcr.2017.04.032

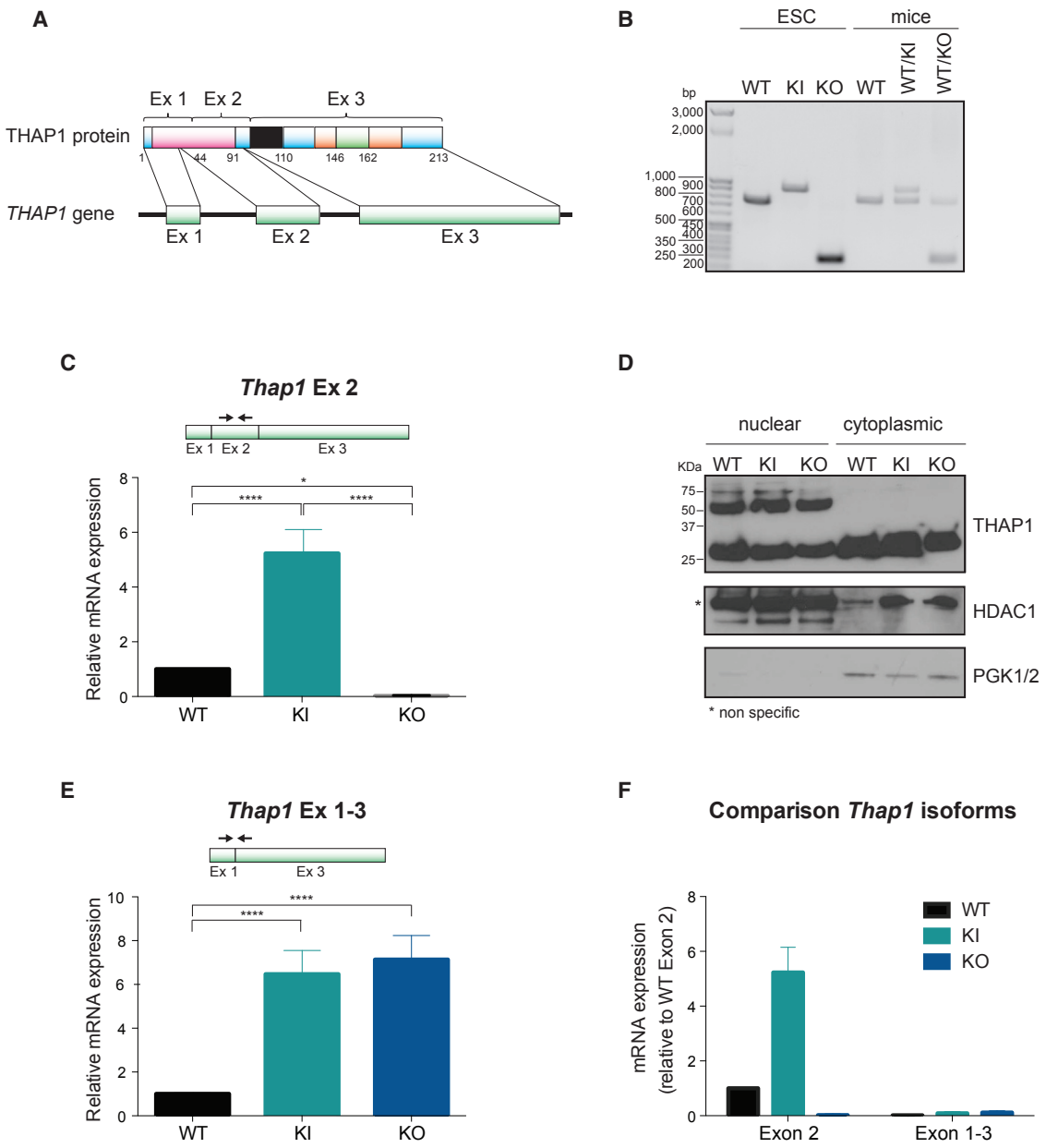

Figure 1. Generation of *Thap1*-Recombinant ESCs

(A) Structure of *Thap1* gene and its encoded protein.

(B) Genotyping of wild-type (WT), $Thap1^{C54Y/C54Y}$ (KI), and $Thap1^{\Delta Exon2}$ (KO) ESCs by PCR and comparison with the pattern of WT, $Thap1^{C54Y/+}$ (WT/KI), and $Thap1^{\Delta Exon2/+}$ (WT/KO) heterozygote mice.

(C) *Thap1* exon 2 (*Thap1* Ex 2) transcript level measured by qRT-PCR in wild-type (WT), $Thap1^{C54Y/C54Y}$ (KI), and $Thap1^{\Delta Exon2}$ (KO) ESCs. An ANOVA was performed which revealed a significant difference among the genotypes ($F(2,23) = 91.69$, $p < 0.001$). The Holm-Sidak multiple comparisons test was performed post hoc, revealing significant differences between the genotypes. Data are presented as mean ± SEM of three independent experiments. *$p < 0.05$; ****$p < 0.001$.

(D) Distribution of THAP1 protein in nuclear and cytoplasmic fraction of wild-type (WT), $Thap1^{C54Y/C54Y}$ (KI) and $Thap1^{\Delta Exon2}$ ESCs (KO). Histone deacetylase 1 (HDAC1) and phosphoglycerate kinase 1/2 (PGK1/2) were used as a control of nuclear and cytoplasmic extract purity, respectively.

(E) Level of *Thap1* transcript spanning exon 1 and exon 3 (*Thap1* Ex 1–3) measured by qRT-PCR in wild-type (WT), $Thap1^{C54Y/C54Y}$ (KI), and $Thap1^{\Delta Exon2}$ (KO) ESCs. ANOVA revealed a significant difference among the genotypes ($F(2,21) = 73.85$, $p < 0.0001$). The Holm-Sidak

(legend continued on next page)

Please cite this article in press as: Aguilo et al., THAP1: Role in Mouse Embryonic Stem Cell Survival and Differentiation, Stem Cell Reports (2017), http://dx.doi.org/10.1016/j.stemcr.2017.04.032

apparently for terminal neuronal differentiation in C54Y homozygote surviving cells.

RESULTS

Generation of *Thap1*-Recombinant Embryonic Stem Cells

To explore the function of THAP1 in ESCs, we derived ESCs from two mouse alleles, (1) *Thap1*^{C54Y}, a constitutive knockin (KI) of the C54Y causative mutation in the DBD of THAP1, and (2) *Thap1*$^{\Delta Exon2}$, a constitutive knockout (KO), allele lacking exon 2 (Ruiz et al., 2015; Figure 1A). Genotypes of wild-type (WT), *Thap1*$^{C54Y/C54Y}$, and *Thap1* $^{\Delta Exon2/\Delta Exon2}$ ESCs were analyzed by PCR and compared with WT, *Thap1*$^{C54Y/+}$, and *Thap1* $^{\Delta Exon2/+}$ heterozygote mice (Figure 1B). Consistent with THAP1 autorepression (Erogullari et al., 2014) and failure of THAP1^{C54Y} to bind at the *Tor1a* promoter (Gavarini et al., 2010), *Thap1*^{C54Y} cells exhibited higher levels of *Thap1* mRNA than WT ESCs, whereas full-length *Thap1* mRNA was undetectable in *Thap1*$^{\Delta Exon2}$ ESCs (Figure 1C). THAP1 antibodies recognize several THAP1-like immunoreactive (THAP1-LIR) species (Ortiz-Virumbrales et al., 2014). Subcellular fractionation followed by western blot analysis revealed the presence of three distinct THAP1-LIR species in the nuclear fraction at ~29 kDa, ~50 kDa, and ~75 kDa (Figure 1D, upper panel). Only the ~75-kDa species was induced or drastically reduced in *Thap1*^{C54Y} or *Thap1*$^{\Delta Exon2}$ ESCs, respectively, following the same pattern of the corresponding mRNA as assessed by qRT-PCR (Figure 1C). Thus, the ~29- and ~50-kDa species appear to be largely composed of cross-reacting proteins in ESCs. In murine brain, the ~29-kDa species was also non-specific, whereas the 50- and 75-kDa THAP1-LIR species were nuclear and neuron specific, and virtually undetectable in ΔExon2 embryos (Ortiz-Virumbrales et al., 2014). Primers spanning exon 1 and exon 3 of *Thap1* mRNA amplified a de-repressed transcript, i.e., its expression was induced, in *Thap1*$^{C54Y/C54Y}$ and *Thap1*$^{\Delta Exon2}$ ESCs (Figure 1E). This naturally occurring THAP1$^{\Delta Exon2}$ represents less than 1% relative to the major isoform (containing exon 2) (Figure 1F) and in vivo does not substitute for the loss of the full-length isoform.

Loss of THAP1 Alters ESC Viability

To investigate THAP1 function in self-renewal, we analyzed the expression of stage-specific embryonic antigen 1 (SSEA1) and POU5F1 (Palmqvist et al., 2005) in all three genotypes (Figure 2A, top and middle panels). There were no detectable differences. The level of alkaline phosphatase (AP) staining (Figure 2A, bottom panels), characteristic of undifferentiated ESCs, was also genotype independent. These data suggest that THAP1 is not required to maintain the pluripotency state of ESCs.

To assess the proliferation rates of WT, *Thap1*^{C54Y}, and *Thap1*$^{\Delta Exon2}$ ESCs, we counted the cells at predetermined times after plating. *Thap1*^{C54Y} ESC proliferation rate was slightly slower than in WT cells, whereas deletion of THAP1 Exon2 severely compromised proliferation (Figure 2B). Viability was not affected in *Thap1*^{C54Y} ESCs as indicated by annexin V, whereas the number of viable cells was reduced ~25% in *Thap1*$^{\Delta Exon2}$ ESCs compared with WT (Figure 2C). Propidium iodide (PI) staining followed by DNA flow cytometry revealed a significant reduction in G_2/M-phase cell populations and a corresponding increase in the number of cells in S phase (Figure 2D) in the *Thap1*$^{\Delta Exon2}$ ESCs. Again, *Thap1*^{C54Y} showed no significant differences compared with WT ESCs. Thus, loss of full-length THAP1, but not the C54Y mutation, affects cell viability by increasing the rate of cell death and arresting the cell cycle at the S phase.

Global Expression Profile of *Thap1*^{C54Y} and *Thap1*$^{\Delta Exon2}$ ESCs

We studied the global transcriptional response in both ESC lines via high-throughput RNA sequencing (RNA-Seq), and identified a larger number of differentially regulated genes in *Thap1*$^{\Delta Exon2}$ than in *Thap1*^{C54Y} ESCs (Figure 3A and Table S1). Specifically, comparing *Thap1*^{C54Y} with WT ESCs, there were 391 upregulated and 163 downregulated genes, whereas comparing *Thap1*$^{\Delta Exon2}$ with WT we identified 1,245 upregulated and 1,237 downregulated genes (Figure 3A). Notably, 93% of the upregulated and 89.5% of the downregulated *Thap1*^{C54Y} genes were common to both genotypes (Figure 3B), but a heatmap illustrated that *Thap1*^{C54Y} and *Thap1*$^{\Delta Exon2}$ alleles have distinct effects on the transcriptional ESC profile (Figure 3C). These differences were also reflected by gene ontology (GO) analyses of biological processes of uniquely differentially expressed genes (Figure S1), and could not be attributed to metabolic or apoptotic gene expression dysregulation. Interestingly, GO analyses of biological processes of upregulated genes ($\log_2$ fold change = +1 of the *Thap1*$^{\Delta Exon2}$ ESC dataset) revealed categories related to embryonic pattern specification, synapsis, chromosome organization, meiosis, and negative regulation of cell differentiation (Figure 3D,

multiple comparisons test was performed post hoc, revealing significant differences between the genotypes. Data are presented as mean ± SEM of at least three independent experiments. ****p < 0.001.

(F) Comparison of *Thap1* isoforms by qRT-PCR in wild-type (WT), *Thap1*$^{C54Y/C54Y}$ (KI), and *Thap1*$^{\Delta Exon2}$ (KO) ESCs. Data are presented as mean ± SEM.

Please cite this article in press as: Aguilo et al., THAP1: Role in Mouse Embryonic Stem Cell Survival and Differentiation, Stem Cell Reports (2017), http://dx.doi.org/10.1016/j.stemcr.2017.04.032

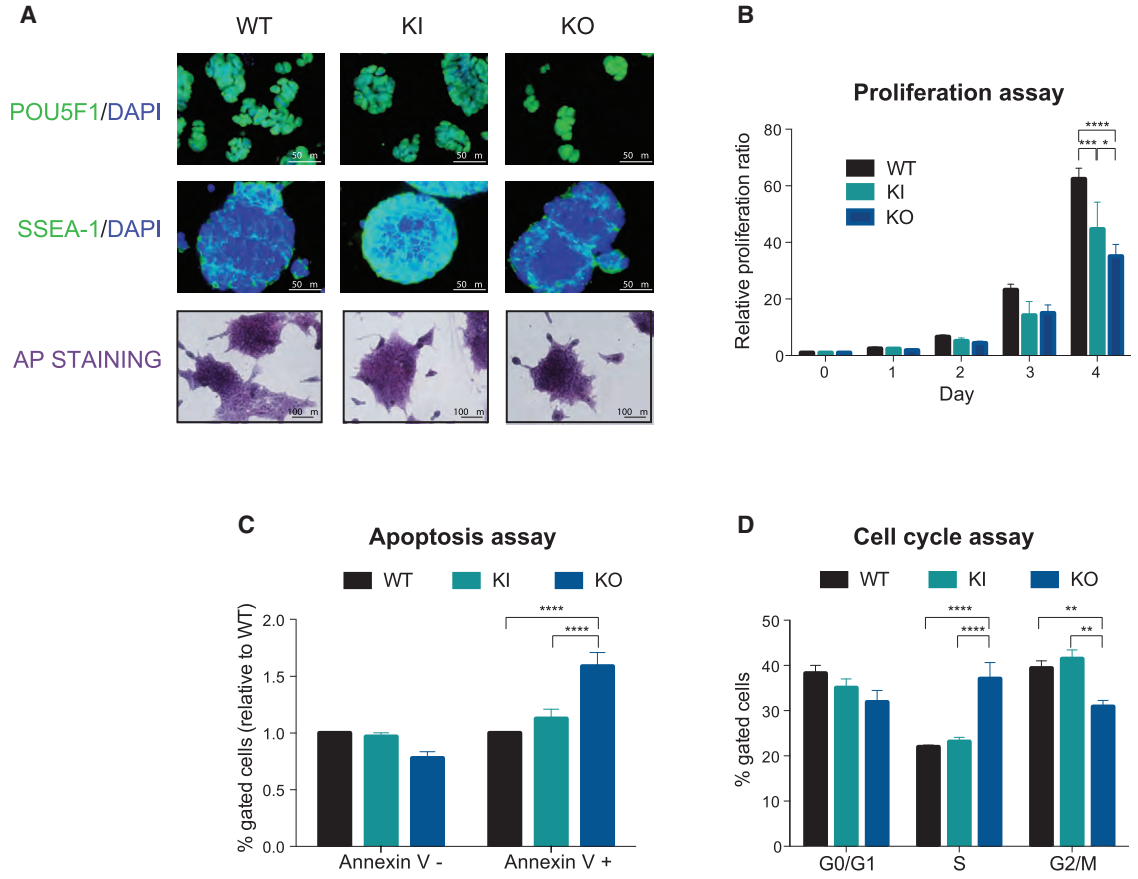

Figure 2. THAP1 Is Not Required for ESC Maintenance

(A) Immunofluorescence analysis of POU5F1 (upper panel) SSEA1 (middle panel), and alkaline phosphatase (AP) staining (lower panel) in wild-type (WT), *Thap1*$^{C54Y/C54Y}$ (KI), and *Thap1*$^{\Delta Exon2}$ (KO) ESCs.

(B) Proliferation rate of wild-type (WT), *Thap1*$^{C54Y/C54Y}$ (KI), and *Thap1*$^{\Delta Exon2}$ (KO) ESCs relative to day 0 and measured by counting the cells at the indicated time points. Two-way repeated-measure (RM) ANOVA was performed revealing an interaction effect between days and genotype ($F(8,36) = 4.288$, $p = 0.0011$). In addition, significant differences were observed by day ($F(4,36) = 139.4$, $p < 0.0001$), while marginal differences were observed by genotype ($F(2,9) = 3.685$, $p = 0.0677$). The Holm-Sidak multiple comparisons test was performed post hoc, revealing significant differences between the genotypes. Data are presented as mean ± SEM of four independent experiments. *$p < 0.05$, ***$p < 0.005$, ****$p < 0.001$.

(C) Percentage of live (Annexin V−) and dead cells (Annexin V+) in wild-type (WT), *Thap1*$^{C54Y/C54Y}$ (KI), and *Thap1*$^{\Delta Exon2}$ (KO) ESCs relative to WT. Two-way RM ANOVA was performed revealing an interaction effect ($F(2,24) = 21.29$, $p < 0.0001$). In addition, significant differences were observed by apoptotic marker ($F(4,36) = 139.4$, $p < 0.0001$) and by genotype ($F(2,24) = 4.205$, $p = 0.0272$). The Holm-Sidak multiple comparisons test was performed post hoc, revealing significant differences between the genotypes. Data are presented as mean ± SEM of five independent experiments. ****$p < 0.001$.

(D) Cell-cycle distribution of wild-type (WT), *Thap1*$^{C54Y/C54Y}$ (KI), and *Thap1*$^{\Delta Exon2}$ (KO) ESCs relative examined by DNA content index. Two-way RM ANOVA was performed, revealing an interaction effect ($F(4,48) = 14.61$, $p < 0.0001$). In addition, significant differences were observed by cell-cycle phase ($F(2,48) = 21.52$, $p < 0.0001$), but not by genotype. The Holm-Sidak multiple comparisons test was performed post hoc, revealing significant differences between the genotypes for S and G_2/M cell-cycle phases. Data are presented as mean ± SEM of four independent experiments. **$p < 0.01$, ****$p < 0.001$.

upper panel). Analysis of downregulated genes (log_2 fold change = −1 of the *Thap1*$^{\Delta Exon2}$ ESC dataset) demonstrated enrichment for processes involved in neuron development, including neuron differentiation, axon guidance, axonogenesis, and cell projection organization (Figure 3D, lower panel). Known pluripotency genes, including *Rex1*, *Prdm14*, and *Nanog* were increased in both *Thap1*^{C54Y} and *Thap1*$^{\Delta Exon2}$ ESCs, whereas *Klf4*, *Esrrb*, and *Pou5F1* were increased only in *Thap1*$^{\Delta Exon2}$ ESCs, all compared with WT ESCs (Figure 3E). In contrast, ectodermal markers, e.g., *Gbx2* and *Sox11*, were decreased in *Thap1*^{C54Y} ESCs, and *Pax6*, *Sox11*, *Olig2*, and *Fgf5* were decreased in *Thap1*$^{\Delta Exon2}$

Please cite this article in press as: Aguilo et al., THAP1: Role in Mouse Embryonic Stem Cell Survival and Differentiation, Stem Cell Reports (2017), http://dx.doi.org/10.1016/j.stemcr.2017.04.032

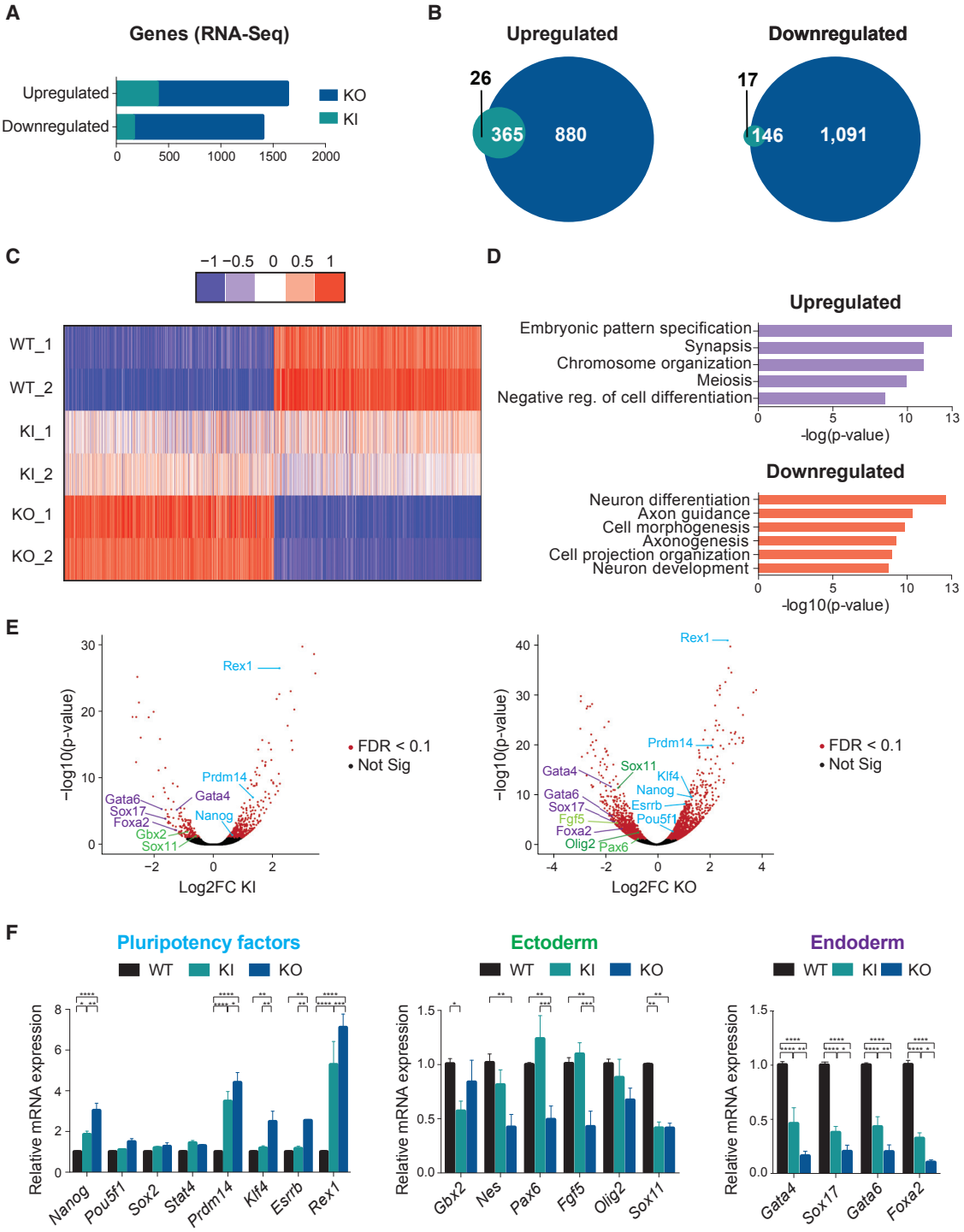

Figure 3. THAP1 Negatively Regulates the ESC Transcriptome

(A) Bar graph illustrating the numbers of upregulated and downregulated genes in *Thap1*$^{C54Y/C54Y}$ (KI) and *Thap1*$^{\Delta Exon2}$ (KO) compared with wild-type (WT) ESCs by RNA sequencing (RNA-Seq).

(B) Venn diagram showing the overlap of upregulated (left panel) and downregulated (right panel) genes in *Thap1*$^{C54Y/C54Y}$ (KI) and *Thap1*$^{\Delta Exon2}$ (KO) ESCs.

(C) Heatmap illustrating the global gene expression performed in duplicates of wild-type 1 and 2 (WT_1 and WT_2), *Thap1*$^{C54Y/C54Y}$ 1 and 2 (KI_1 and KI_2), and *Thap1*$^{\Delta Exon2}$ 1 and 2 (KO_1 and KO_2) ESCs.

(legend continued on next page)

ESCs, all compared with WT. Endoderm specification genes, including *Gata4*, *Gata6*, *Sox17*, and *Foxa2*, were also significantly decreased in both genotypes compared with WT ESCs (Figure 3E), whereas no differences in mesoderm markers were detected (data not shown). The RNA-Seq results were confirmed by qRT-PCR for selected genes (Figure 3F). Altogether, these results provide initial evidence that pluripotency factors and developmental regulators are differentially, and oppositely, regulated after C54Y mutation of *Thap1*, and that such changes in the ESC transcriptome are even more apparent after loss of full-length THAP1.

THAP1 Genomic Binding Analysis

To gain an overview of the global role of THAP1 in ESCs, we performed chromatin immunoprecipitation followed by massively parallel sequencing (ChIP-Seq). We identified 1,731 high-confidence peaks bound by THAP1, corresponding to 1,052 target genes (Table S2), 65 of which were upregulated and 43 were downregulated in $Thap1^{\Delta Exon2}$ ESCs (Figure 4A). THAP1 binding was enriched at the transcription start site (TSS), extending over a 2-kb interval (Figure 4B). THAP1 bound only slightly more at promoters (27.04%) than in intergenic regions (24.10%) (Figure 4C). We used public ESC ChIP-Seq datasets for p300, Med1, and monomethylated histone H3 Lys4 (H3K4me1), acetyl histone H3 Lys27 (H3K27ac), and trimethylated histone H3 Lys27 (H3K27me3) (Arnold et al., 2013; Heintzman et al., 2007, 2009; Rada-Iglesias et al., 2011; Visel et al., 2009) to determine that THAP1 occupation was detected at activated enhancers but not with the H3K27me3 silent mark (Figure 4D). By clustering the ChIP-Seq enrichment profiles of RNA polymerase II Ser-5 phosphorylated (Pol II Ser-5P) and the histone modification trimethylated histone H3 Lys4 (H3K4me3) with high-confidence THAP1 peaks, we found that THAP1 occupancy occurred at promoter regions of activated genes (Figure 4E) associated with GO categories related to metabolic processes, including nucleobase-containing compound and RNA metabolic, and neurologic system process (Figures 4F and S2A). THAP1 also occupied bivalent or poised genes that are associated with developmental processes, system development, cell communication, and nervous system and ectoderm development, among others (Figures 4F and S2B). Occupancy of THAP1 at silent genes was related to diverse functions, including developmental and immune system process (Figures 4F and S2C). We identified the top DNA motifs enriched at the THAP-domain-binding sequence (THABS) and de novo motifs using the top 1,000 THAP1 peaks and the algorithm MEME (Figure 4G, left panel). Motifs #1 and #3 overlapped with the THABS identified by ENCODE in the human K562 cell line (Kheradpour and Kellis, 2014). Motif #3 contained the core GGCA sequence, essential for recognition by the THAP domain (Clouaire et al., 2005). Secondary motifs overrepresented in THABS overlapped with the binding sequence for RE-silencing transcription factor (REST), which represses the expression of neuronal genes in differentiated non-neuronal cells (Ballas et al., 2005), and Yin Yang 1 (YY1), which plays multiple roles in the development of the central and peripheral nervous systems (He and Casaccia-Bonnefil, 2008; Figure 4G, right panel). Consistent with previous reports, inspection of individual gene tracks showed THAP1 binding at the core promoter of *Thap1* and *Tor1A* (Erogullari et al., 2014; Gavarini et al., 2010; Kaiser et al., 2010), thus validating our approach (Figures 5A and 5B, left panel). ChIP-qPCR using anti-THAP1 antibody confirmed THAP1 occupancy at these sites in WT but not in $Thap1^{C54Y}$ and $Thap1^{\Delta Exon2}$ ESCs (Figures 5A and 5B, right panel), and at promoters of the cell-cycle genes Aurora A kinase (*Aurka*) and tumor protein p53 (*Trp53*), at the apoptosis genes Bcl-2-associated death promoter (*Bad*) and DNA fragmentation factor subunit beta (*Dffb*), and at the splicing factor 3a subunit 2 (*Sf3a2*). Despite this occupancy, the expression of these genes is not altered in $Thap1^{C54Y}$ and $Thap1^{\Delta Exon2}$ ESCs

(D) Gene ontology (GO) analyses of biological processes of the top (log_2 fold change 1) upregulated (upper panel) and downregulated (lower panel) genes of the $Thap1^{\Delta Exon2}$ ESCs dataset.

(E) Volcano plots demonstrated differentially expressed genes in $Thap1^{C54Y/C54Y}$ (KI) (left panel) and $Thap1^{\Delta Exon2}$ (KO) (right panel) ESCs versus WT ESCs. Significant and not significant hits are shown in red and black, respectively (false discovery rate [FDR] < 0.1). Pluripotency-associated transcripts are shown in blue. Selected ectoderm and mesoderm RNAs are depicted in green and purple, respectively.

(F) qRT-PCR analysis of selected pluripotency factors (left panel), ectoderm (middle panel), and endoderm (right panel) specification markers in WT, $Thap1^{C54Y/C54Y}$ (KI), and $Thap1^{\Delta Exon2}$ (KO) ESCs. For pluripotency factors, two-way ANOVA was performed, revealing an interaction effect ($F(14,170) = 10.92$, $p < 0.0001$). In addition, significant differences were observed by pluripotency gene(s) ($F(7,170) = 38.54$, $p < 0.0001$) and by genotype ($F(2,170) = 85.22$, $p < 0.0001$). For ectodermal markers, two-way ANOVA was performed, revealing an interaction effect ($F(10,107) = 3.178$, $p = 0.0013$). In addition, marginal differences were observed by ectodermal gene(s) ($F(5,107) = 2.144$, $p = 0.0657$), and significant differences were observed by genotype ($F(2,170) = 22.47$, $p < 0.0001$). For endodermal markers, two-way ANOVA was performed, revealing significant differences by genotype ($F(2,81) = 194.2$, $p < 0.0001$); however, no significant differences were observed by endodermal gene(s), and there was no interaction effect. The Holm-Sidak multiple comparisons test was performed post hoc, revealing significant differences between the genotypes for the following genes: *Nanog*, *Prdm14*, *Klf4*, *Esrrb*, *Rex1*, *Gbx2*, *Nes*, *Pax6*, *Fgf5*, *Sox11*, *Gata4*, *Sox17*, and *Foxa2*. Data are presented as mean ± SEM of four independent experiments. *$p < 0.05$, **$p < 0.01$, ***$p < 0.005$, ****$p < 0.001$.

Please cite this article in press as: Aguilo et al., THAP1: Role in Mouse Embryonic Stem Cell Survival and Differentiation, Stem Cell Reports (2017), http://dx.doi.org/10.1016/j.stemcr.2017.04.032

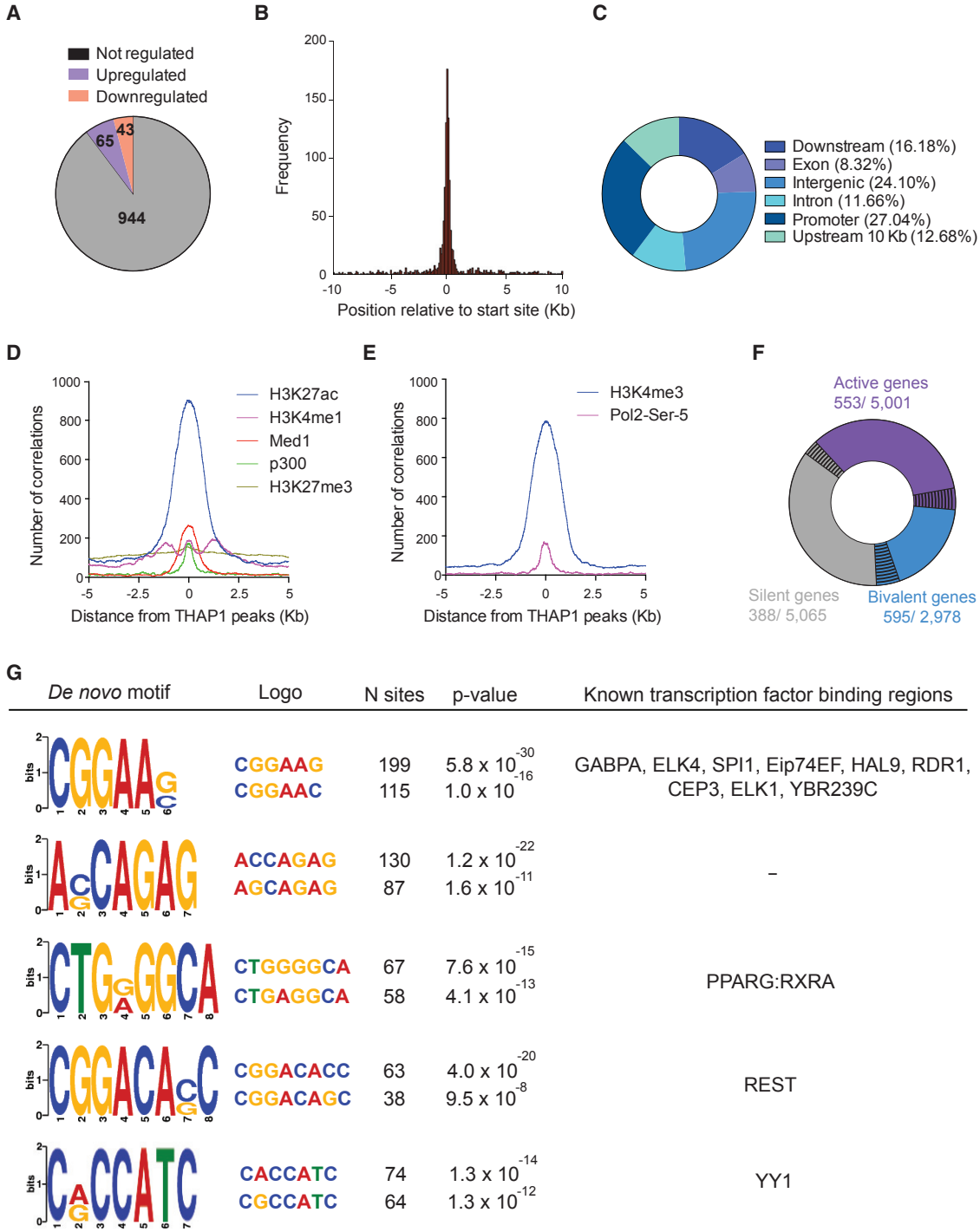

Figure 4. THAP1 ChIP-Seq Analysis

(A) Pie chart depicting the number of THAP1 only bound genes, activated and bound, and repressed and bound in *Thap1*$^{\Delta Exon2}$ (KO) ESCs.

(B) Histogram showing the distribution of THAP1-binding peaks relative to the nearest TSS.

(C) Pie chart of the genomic distribution of THAP1-binding peaks including promoters (within 5 kb upstream of TSS), downstream (within 10 kb downstream of the gene), introns, exons, upstream (within 10 kb upstream of the gene), and intergenic regions.

(D) p300, MED1, H3K4me1 (characteristic of predicted enhancer), H3K27ac (active state), and H3K27me3 (repressed state) occupancy around the summit of THAP1 peaks.

(legend continued on next page)

compared with WT (Table S1), suggesting that THAP is present on specific promoters as part of an inactive complex poised to respond to defined developmental stimuli yet to be elucidated. Binding of THAP1 at the non-specific region of chromosome 8 was not detected (Figure 5C).

Thap1^{C54Y} and *Thap1*$^{\Delta Exon2}$ EBs Show Increased Cell Death and Fail to Properly Differentiate

To study lineage specification, we assayed EB formation and differentiation (Höpfl et al., 2004). The absence of leukemia inhibitory factor (LIF), replacement of fetal calf serum (FCS) with KnockOut serum replacement, and growth in suspension triggered cell differentiation. WT, *Thap1*^{C54Y}, and *Thap1*$^{\Delta Exon2}$ ESCs formed EB aggregates (Figure S3A). It was immediately apparent that *Thap1*$^{\Delta Exon2}$ EBs were smaller and all died between days 12 and 16. We assayed mRNA levels of markers that either promote or inhibit cell death (Youle and Strasser, 2008). Compared with WT, the expression of *Bax* was higher in *Thap1*^{C54Y} and *Thap1*$^{\Delta Exon2}$ EBs, and *Puma* also increased in the latter, with a peak at day 8 observed in both genotypes (Figure S3B, upper panel). The expression of the anti-apoptotic markers *Xiap* and *Bcl-2* was also higher in *Thap1*$^{\Delta Exon2}$ EBs compared with *Thap1*^{C54Y} and WT EBs, with a striking 50- to 75-fold upregulation of Bcl-2 in *Thap1*$^{\Delta Exon2}$ EBs (Figure S3B, lower panel). Cell viability in EBs was actually decreased in both *Thap1*^{C54Y} and *Thap1*$^{\Delta Exon2}$ ESCs compared with WT ESCs as indicated by annexin V (Figure 6A) and TUNEL staining (Figure 6B), and cleaved caspase-3 staining (Figure S4A), more so in the ΔExon2 EBs. Cell death was not diminished in either genotype when EBs were grown in 40 μM Z-VAD-FMK, a pan-caspase inhibitor (Figure S4B). *Thap1*$^{\Delta Exon2}$ EBs demonstrated the highest percentage of cell death whereas an intermediate level was observed in *Thap1*^{C54Y} EBs, compared with WT, over the 4-day period (Figure S4B). Failure of Z-VAD-FMK to preserve survival is consistent with literature showing that cellular commitment to apoptosis occurs at the level of BCL-2 family-regulated mitochondrial outer membrane permeabilization (i.e., cytochrome *c* release), and that subsequent death phenotypes occur whether or not caspases activate (Chipuk and Green, 2005).

We also used qRT-PCR to assay the expression of differentiation markers in EBs, representing the three germ layers, many of which were already dysregulated in the ESCs. *Thap1* mRNA levels were constant in WT EBs up to day 16, the last day examined. In *Thap1*^{C54Y} ESCs, *Thap1* mRNA was higher than in WT, and increased steadily up to day 16. *Thap1* mRNA was undetectable in *Thap1*$^{\Delta Exon2}$ EBs (Figure 6C, top left panel). The expression of ESC genes *Prdm14* and *Rex1* increased progressively between day 1 and day 12 in *Thap1*$^{\Delta Exon}$ EBs, and the latter also progressively increased in *Thap1*^{C54Y} EBs (Figure 6C, top right panel), suggesting that failure to silence pluripotency genes during differentiation may contribute to restriction of developmental potential. *Thap1*^{C54Y} and *Thap1*$^{\Delta Exon2}$ EBs expressed markers of endodermal lineage (Figure S3C, upper panel) following a pattern similar to that of WT EBs. However, the expression of the mesodermal markers *T* (i.e., *Brachyury*) and *Flk1* was abnormal in the *Thap1*^{C54Y} and *Thap1*$^{\Delta Exon2}$ EBs (Figure S3C, lower right panel). Consistent with the GO analysis, the expression of the ectodermal markers *Sox11*, *Nestin*, and *Tuj1* were decreased in *Thap1*^{C54Y} and *Thap1*$^{\Delta Exon2}$ EBs, whereas the marker of primitive ectoderm *Fgf5* was normally expressed in Thap1$^{C54Y/C54Y}$ and *Thap1*$^{\Delta Exon2}$ EBs compared with WT EBs (Figure S3C, lower panel). Failure of *Thap1*^{C54Y} to increase expression of Tuj1 suggests a stall at early ectodermal differentiation.

THAP1 Is Essential for Neural Differentiation of Mouse ESCs

To further investigate the role of THAP1 during neural differentiation of mESCs from EBs, we used one protocol based on retinoic acid (RA)-dependent neural differentiation (Figure 7A, protocol #1; Okada et al., 2004), and a second protocol without RA but with the addition of N2 supplemented with epidermal growth factor β and insulin (Figure S5A, protocol #2; Okabe et al., 1996). Survival of mutant cells, particularly ΔExon2, was improved in protocol #2 relative to #1. Using protocol #1, undifferentiated, neural progenitor Nestin-positive cells were detected in *Thap1*^{C54Y} EBs, but at a lower expression level than in protocol #2, which has a longer culture period. Using protocol #2, Nestin was detected in both WT and *Thap1*^{C54Y} differentiated cells, but TuJ1-positive neuronal projections, indicative of more mature neurons, were detected almost exclusively in WT ESCs and were abnormally restricted to the internal portion of cell mass in *Thap1*^{C54Y} ESCs, again consistent with a stall at early ectodermal differentiation (Figure S5B). *Thap1*$^{\Delta Exon2}$ EBs failed to develop Nestin- or TuJ1-immunopositive neuronal projections with either

(E) Pol II Ser-5P and H3K4me3 (characteristic of promoters) occupancy around the summit of THAP1 peaks.
(F) Pie chart depicting THAP1 binding sites (black lines) at active (purple), bivalent (blue), and silent (gray) genes (defined in Experimental Procedures).
(G) The top 1,000 TF ChIP-Seq peaks were used to identify THAP1 de novo motif (left panel showing the five most significant motifs) and overlapping of THAP1 binding with the indicated transcription factors (right panel). Number (N) of sites and the corresponding p values are indicated.

Please cite this article in press as: Aguilo et al., THAP1: Role in Mouse Embryonic Stem Cell Survival and Differentiation, Stem Cell Reports (2017), http://dx.doi.org/10.1016/j.stemcr.2017.04.032

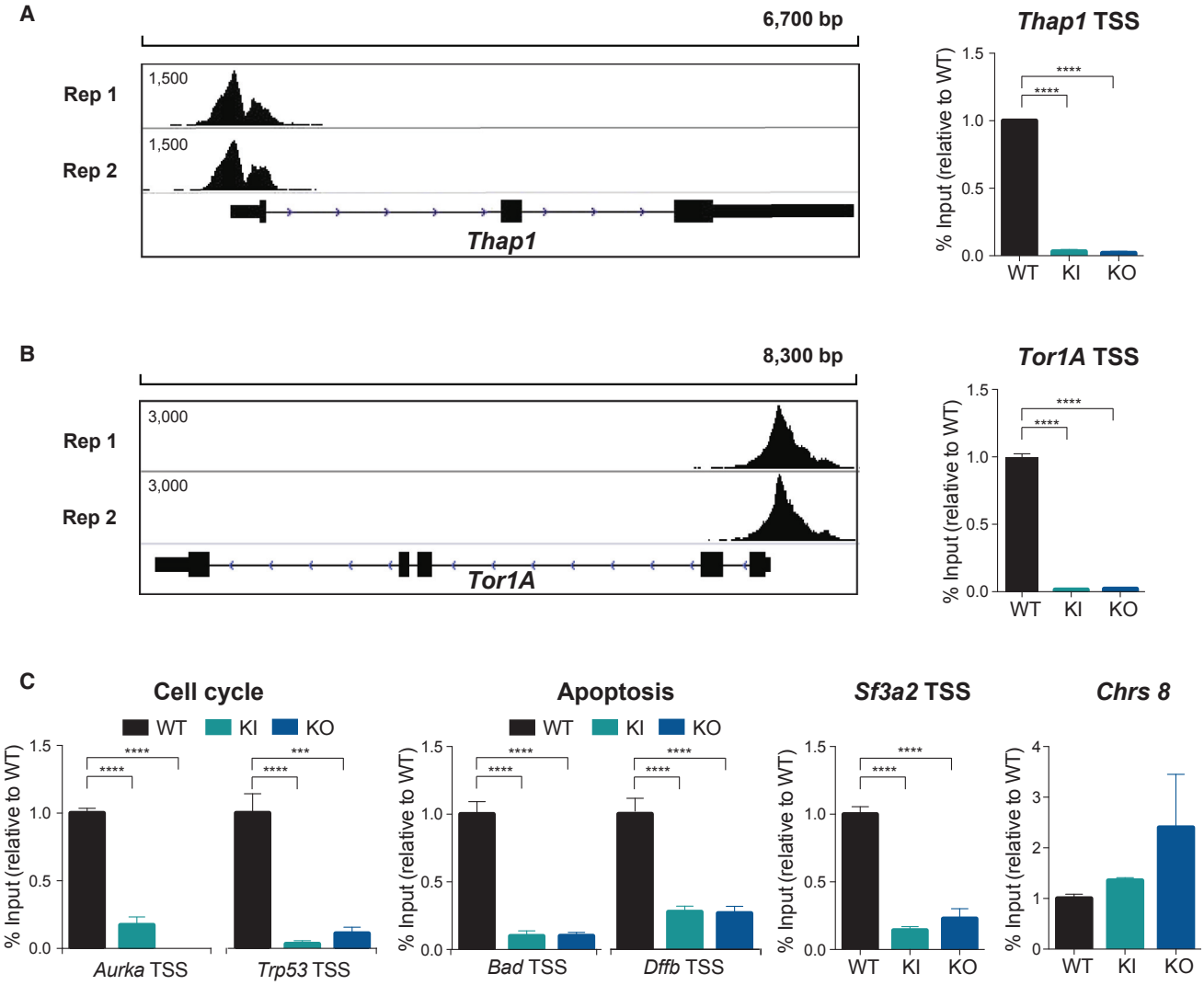

Figure 5. ChIP and qRT-PCR Validation of THAP1 Target Genes

(A) ChIP-Seq binding profiles for THAP1 replicates (Rep) 1 and 2 at the *Thap1* locus (left panel). ChIP qRT-PCR analysis of THAP1 at *Thap1* TSS in WT, *Thap1*$^{C54Y/C54Y}$ (KI), and *Thap1*$^{\Delta Exon2}$ (KO) ESCs (right panel). Data are normalized to percent input and relative to WT. An ANOVA was performed, which revealed a significant difference among the genotypes when examining THAP1 binding ($F(2,8) = 1544$, $p < 0.0001$). Holm-Sidak's multiple comparisons test was performed post hoc, revealing significant differences between the genotypes. Data are presented as mean ± SEM of four independent experiments. ****$p < 0.001$.

(B) ChIP-Seq binding profiles for THAP1 replicates (Rep) 1 and 2 at the *Tor1A* locus (left panel). ChIP qRT-PCR analysis of THAP1 at *Tor1A* TSS in WT, *Thap1*$^{C54Y/C54Y}$ (KI), and *Thap1*$^{\Delta Exon2}$ (KO) ESCs (right panel). Data are normalized to percent input and relative to WT. An ANOVA was performed, which revealed a significant difference among the genotypes when examining THAP1 binding ($F(2,0) = 1854$, $p < 0.0001$). The Holm-Sidak multiple comparisons test was performed post hoc, revealing significant differences between the genotypes. Data are presented as mean ± SEM of four independent experiments. ****$p < 0.001$.

(C) ChIP-qPCR analysis of THAP1 at cell-cycle genes (*Aurka* and *Trp53*), apoptosis (*Bad* and *Dffb*), and *Sf3a2* TSS in WT, *Thap1*$^{C54Y/C54Y}$ (KI), and *Thap1*$^{\Delta Exon2}$ (KO) ESCs. Chromosome 8 was used as a negative control. Data are normalized to percent input and relative to WT. Significant differences were observed among the genotypes when examining the binding of THAP1 at the cell-cycle genes *Aurka* ($F(2,7) = 118.2$, $p < 0.0001$) and *Trp53* ($F(2,9) = 37.43$, $p < 0.0001$). Significant differences were observed among the genotypes when examining the THAP1 binding at apoptosis related genes *Bad* ($F(2,9) = 74.64$, $p < 0.0001$) and *Dffb* ($F(2,9) = 39.21$, $p < 0.0001$). Significant differences were observed among the genotypes when examining the THAP1 binding at the RNA splicing related gene, *Sf3a2* ($F(2,9) = 39.21$, $p < 0.0001$). No differences were observed among the genotypes with ANOVA when examining the THAP1 binding at Chrs8. The Holm-Sidak multiple comparisons test was performed post hoc, revealing significant differences between the genotypes. Data are presented as mean ± SEM of four independent experiments. ***$p < 0.005$, ****$p < 0.001$.

Please cite this article in press as: Aguilo et al., THAP1: Role in Mouse Embryonic Stem Cell Survival and Differentiation, Stem Cell Reports (2017), http://dx.doi.org/10.1016/j.stemcr.2017.04.032

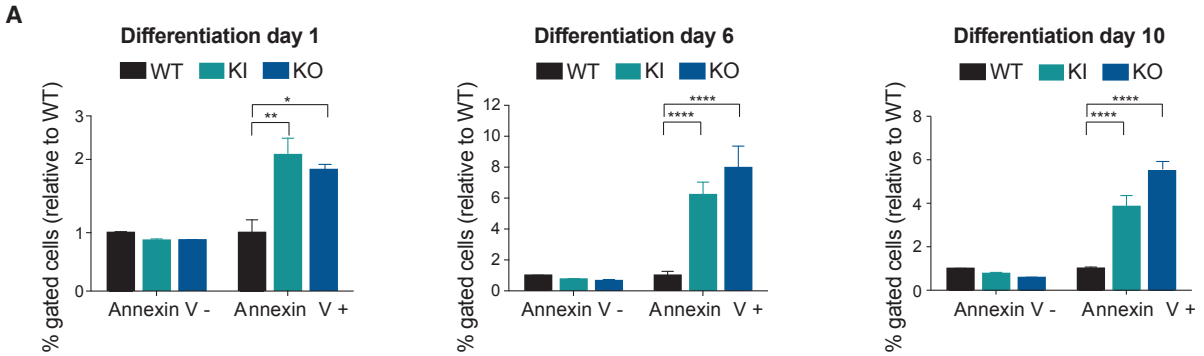

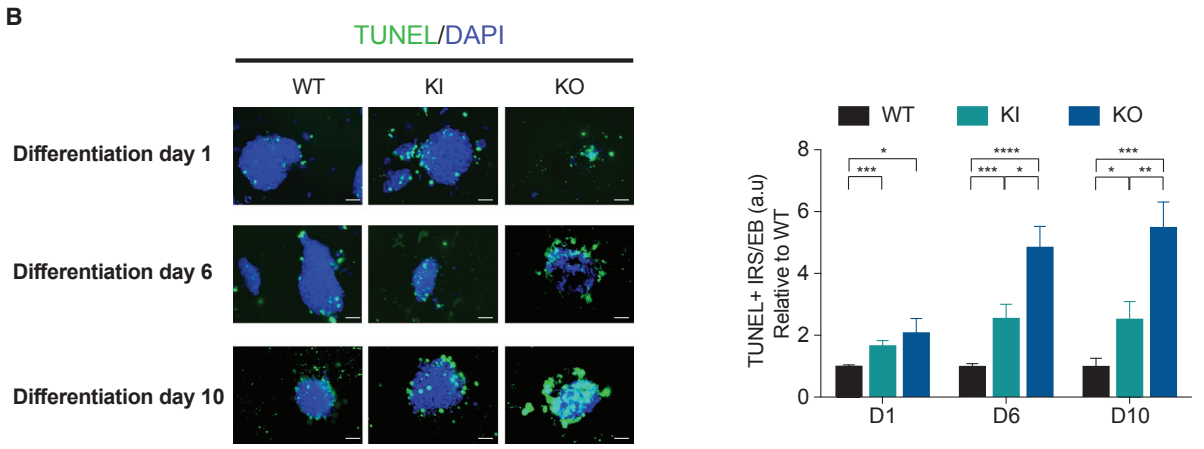

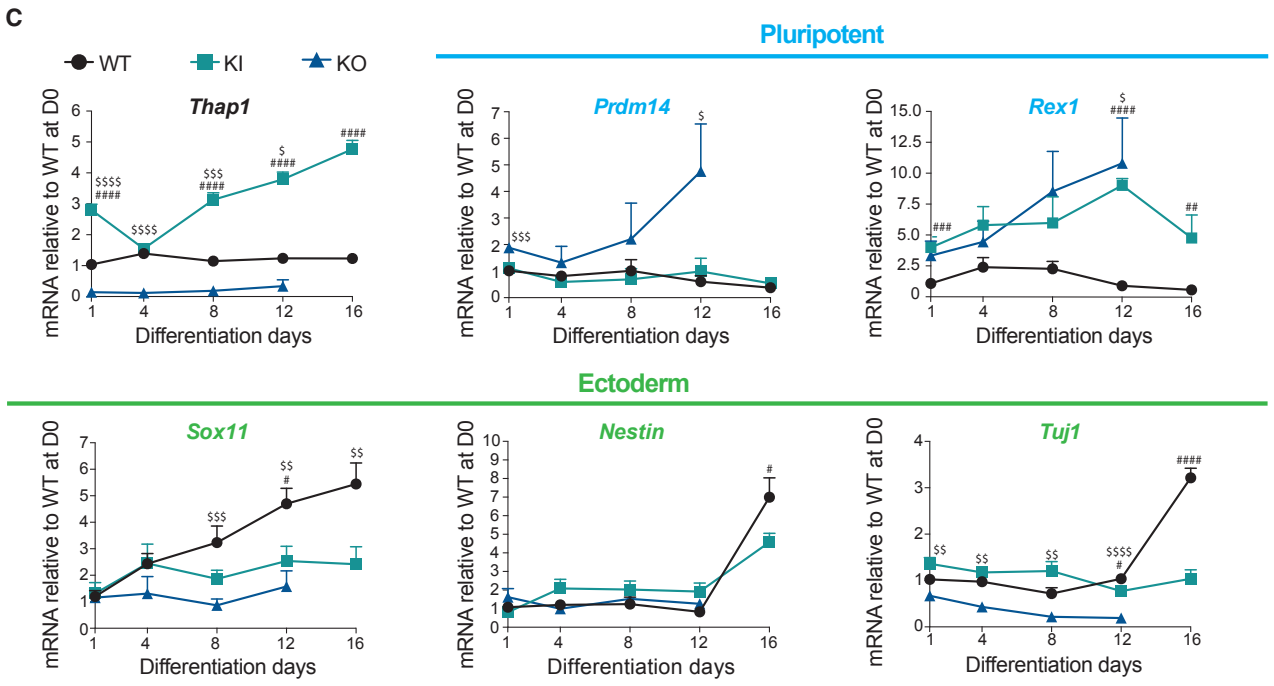

(legend on next page)

Please cite this article in press as: Aguilo et al., THAP1: Role in Mouse Embryonic Stem Cell Survival and Differentiation, Stem Cell Reports (2017), http://dx.doi.org/10.1016/j.stemcr.2017.04.032

protocol (Figures 7B and S5B). The quantification of neuronal projections in the three genotypes is illustrated in the bar graphs (Figures 7C and S5C). Expression of the ESC genes *Prdm14*, *Nanog*, and *Rex1* in samples from protocol #1 (Figure 6) was abnormally enhanced in $Thap1^{C54Y}$ and $Thap1^{\Delta Exon2}$ EBs, even at the later stages of neuronal differentiation (Figure 7D, upper panel). We also monitored progression of ESC differentiation toward neural fates by analysis of *Pax6*, *Sox11*, *Nestin*, and *Tuj1* expression with qRT-PCR. $Thap1^{C54Y}$ and $Thap1^{\Delta Exon2}$ failed to activate the expression of these ectodermal markers, suggesting a role for THAP1 in multiple stages of neuronal differentiation (Figure 7D, lower panel). Similar results were obtained by expression analysis in protocol #2 (Figure S5D). Collectively, our results show that THAP1 is required to silence the expression of the pluripotency factors and to activate the expression of the neural factors (Figure 7E).

DISCUSSION

We have identified THAP1 as a major regulator of ESC survival and, to a lesser degree, proliferation and differentiation. As *THAP1* mutations result in a neurologic disease, we were particularly interested in the effects of a causative mutation, C54Y, on neuronal differentiation. We had previously posited, based on observations of homozygote mutant embryos, that THAP1 is required in multiple stages and layers during embryogenesis, organogenesis, and maturation of the nervous system, including neurogenesis and neuritogenesis, and that the C54Y variant is frequently unable to substitute for the WT (Ruiz et al., 2015).

In all assays, the homozygous ΔExon2 phenotype was more severe than that of the homozygous C54Y phenotype, confirming that C54Y does not confer a complete loss of function. Both genotypes showed a decreased rate of proliferation, more so in the ΔExon2, consistent with regulation of the cell cycle by THAP1 in HUVECs and lymphoblasts (Cayrol et al., 2007; Vemula et al., 2014). Only the ΔExon2 homozygote showed a decrease in viability in the ESC stage. Thus, a loss of WT THAP1 promotes cell death even though THAP1 is reportedly a pro-apoptotic factor (Roussigne et al., 2003). The lack of a requirement for THAP1 for pluripotency is in marked contrast to RONIN/THAP11, another member of the THAP family to have been characterized in this manner (Dejosez et al., 2008).

We compared this study of the global transcriptome in ESCs harboring a mutation of THAP1 with previous microarray assays of HUVECs with up- or downregulation of THAP1 and of human lymphoblasts harboring a disease-causing intronic variant of *THAP1*, both of which revealed that the main pathway regulated by THAP1 is the cell cycle. The cell-cycle abnormalities and cell death described herein bear a strong resemblance to these HUVECs and lymphoblasts. Similar to the $Thap1^{\Delta Exon2}$ ESCs, the mutant human lymphoblastoid cells had decreased viability and showed a reduced number of cells in the G_2 phase (Vemula et al., 2014). In HUVECs, knockdown of *THAP1* resulted in an impaired G_1/S phase (Cayrol et al., 2007). Despite the presence of cell-cycle abnormalities in the *THAP1* null cells, cell-cycle genes were not a highly ranked GO category, but genes pertaining to meiosis and X chromosome inactivation categories were also differentially expressed in $Thap1^{C54Y/C54Y}$ and $Thap1^{\Delta Exon2}$ compared with WT ESCs.

We examined the role of THAP1 in ESC differentiation by performing EB formation assays. EB formation and growth were highly compromised in $THAP1^{\Delta Exon2}$ cells. Indeed, we

Figure 6. $Thap1^{C54Y/C54Y}$ and $Thap1^{\Delta Exon2}$ ESCs Show Abnormal EB Viability and Differentiation

(A) Percentage of live (Annexin V−) and apoptotic cells (Annexin V+) were measured over EB differentiation days 1, 6, and 10 in wild-type (WT), $Thap1^{C54Y/C54Y}$ (KI), and $Thap1^{\Delta Exon2}$ (KO) EBs. On each day, data (mean ± SEM) are presented relative to WT = 1. The two-way ANOVA results for the annexin V assay during EB differentiation days 1, 6, and 10 can be found in Table S3. Bonferroni's multiple comparisons test was performed post hoc, revealing significant differences between the genotypes for each differentiation day. Data are presented as mean ± SEM of three independent experiments. *p < 0.05; **p < 0.01, ****p < 0.001.

(B) Wild-type (WT), $Thap1^{C54Y/C54Y}$ (KI), and $Thap1^{\Delta Exon2}$ (KO) EBs were examined with TUNEL on differentiation days 1, 6, and 10 (left panel; scale bar, 50 μm). Quantification of $TUNEL^+$ EBs (right panel) was performed by scoring TUNEL-immunopositive cells (immunoreactive species [IRS^+]) as a function of total EB area, normalized to WT for each differentiation day. The two-way ANOVA results for TUNEL IRS^+/EB quantifications during EB differentiation days 1, 6, and 10 can be found in Table S3. Bonferroni's multiple comparisons test was performed post hoc, revealing significant differences between the genotypes for each differentiation day. Data are presented as mean ± SEM; n = 10 per group for each day, with data pooled from three independent experiments. *p < 0.05; **p < 0.01, ***p < 0.005, ****p < 0.001.

(C) qRT-PCR analysis of *Thap1*, pluripotency markers, and ectodermal markers during EB differentiation of $Thap1^{C54Y/C54Y}$ (KI) and $Thap1^{\Delta Exon2}$ (KO) ESCs at the indicated time points. Data are normalized to WT, relative to D1. The two-way ANOVA results for Thap1, pluripotency markers (*Prdm14* and *Rex1*), and ectodermal markers (*Sox11*, *Nestin*, and *Tuj1*) for differentiation days 1, 6, and 10 can be found in Table S3. Bonferroni multiple comparisons test was performed post hoc, revealing significant differences between the genotypes. Data are presented as mean ± SEM of three independent experiments, relative to WT. *p < 0.05; **p < 0.01, ***p < 0.005, ****p < 0.001. # denotes differences between KI versus WT; $ denotes differences between KO versus WT.

Please cite this article in press as: Aguilo et al., THAP1: Role in Mouse Embryonic Stem Cell Survival and Differentiation, Stem Cell Reports (2017), http://dx.doi.org/10.1016/j.stemcr.2017.04.032

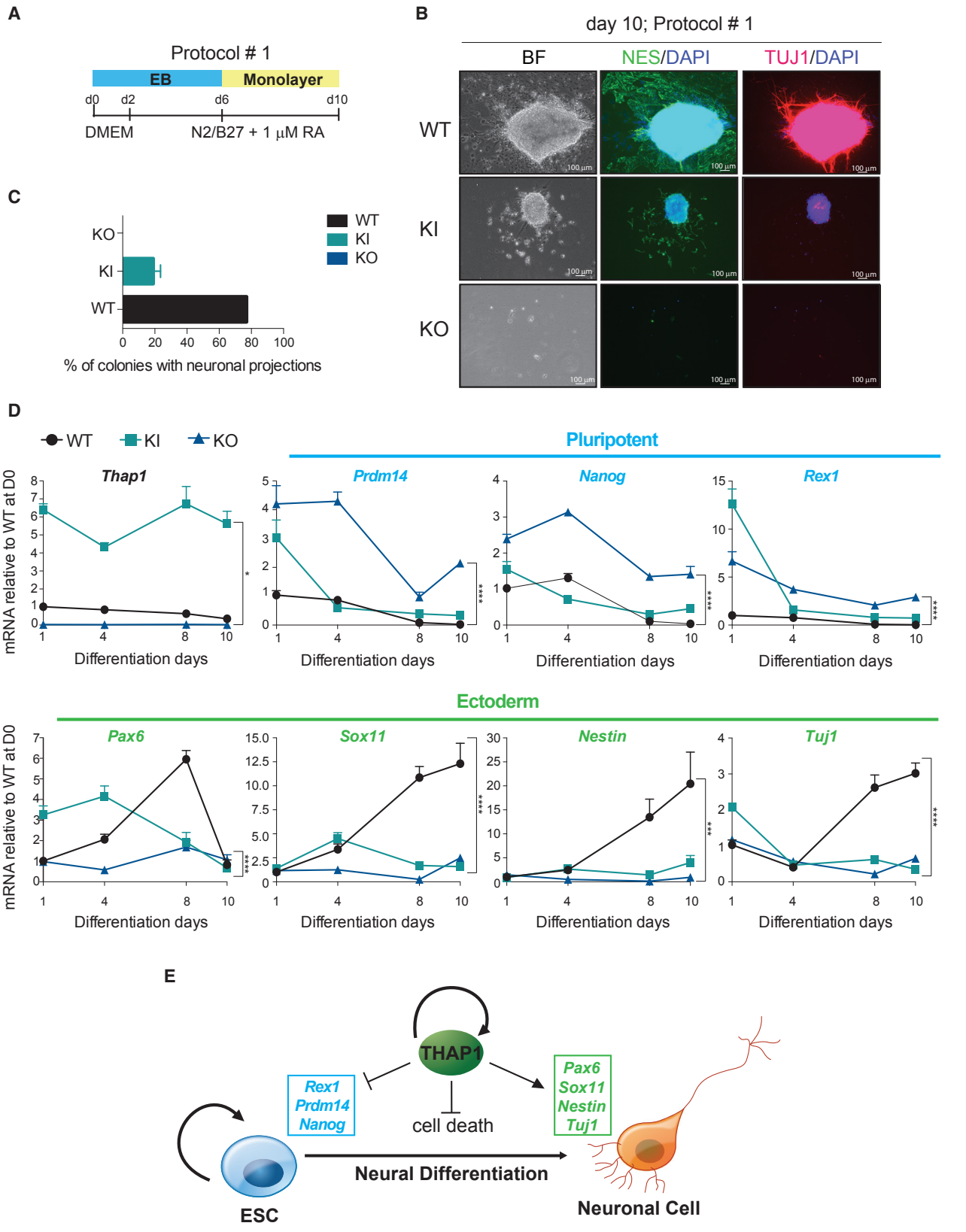

(legend on next page)

showed that cell viability was compromised in both *Thap1*^{C54Y} and *Thap1*$^{\Delta Exon2}$ EBs, with a greater cell death phenotype after loss of full-length THAP1. The extent of cell death in the ΔExon2 EBs precludes a conclusion regarding an effect on differentiation. Our investigations into the mechanism of cell death implicate the mitochondrial pathway of apoptosis as responsible for cell death commitment and caspase activation. Cell death execution, however, apparently can proceed independently of caspase activation. Delineation of a definitive sequence of events leading to cell death requires further characterization. Although there is increased cell death in the *Thap1*^{C54Y} EBs, their survival is sufficient to enable some conclusions regarding differentiation. Specifically, mesoderm specification may be delayed, but, more strikingly for a mutation that leads to a neurologic disease, neuronal differentiation appears to stall at an early stage.

The mechanism(s) via which the *Thap1* mutations prevent repression of pluripotency markers is not entirely obvious, but there are leads, particularly in the categories of dysregulated genes. An in silico search for THABS motifs in mouse *Nanog*, *Prdm14*, *Pou5f1*, *Esrrb*, and *Klf4* was negative, and ChIP-Seq did not uncover binding sites in these genes. Regulation of the pluripotency network requires cooperation between multiple transcription factors, including the pluripotency factors themselves, signal transduction pathways, and epigenetic modifications. Notably, of the DEGs detected by RNA-Seq, many genes in these categories are altered, e.g., *Bmp4*, *Dnmt3a* and *Dnmt3b*, *Satb1*, *Klf10*, *Sirt6*, and *Sox17*, with a greater degree of dysregulation in the *Thap1*$^{\Delta Exon2}$ relative to the *Thap1*^{C54Y} ESCs. Interestingly, *Dnmt3a* and 3b, *Satb1*, and *Sox17* KO ESCs display phenotypes that are similar in many ways to those of the *Thap1* mESCs. Specifically, upon exposure to differentiation factors, they simultaneously fail to downregulate pluripotency genes and upregulate lineage-specific genes, some of which are already decreased prior to differentiation (Bergsland et al., 2011; Chen et al., 2003; Savarese et al., 2009). Thus, the mechanism via which THAP1 regulates these genes requires further examination but may represent a pathway for inverse regulation of pluripotency and differentiation genes.

The low percentage (10%) of overlap between RNA-Seq and ChIP-Seq datasets suggests an alternative role of THAP1 in regulating gene expression other than direct binding at DNA, as exists with other zinc-finger factors (Aguilo et al., 2015). This conclusion may also be supported by the relatively low $\log_2$ fold changes observed in the *Thap1*^{C54Y} ESCs, as much greater changes are seen in *Thap1*$^{\Delta Exon2}$ ESCs, where the full-length transcription factor is eliminated. It is possible that the mutant THAP1 proteins are able to bind to some, but not all, targets of WT THAP1, and in addition, may bind to sequences that are normally not bound by WT THAP1 (Campagne et al., 2012). Also, these mutant proteins may participate in THAP1 protein interactions. For example, THAP1 interacts with HCF-1 via a motif that does not include amino acid 54 (Mazars et al., 2010). Therefore, the C54Y form may still be able to interact with HCF-1, Par-4, and partners as yet to be identified, thereby recruiting such transcription factors to the target DNA. This hypothesis would be consistent with the fact that there are individuals with dystonia with homozygote *THAP1* mutations. In the case where THAP1 binding is decreased or eliminated, there may be increased binding of transcription factors with an affinity for similar motifs. As noted, these include YY1 and REST, thereby altering levels of their direct and indirect targets, which include many of the RNA-Seq DEGs. In fact, there is a very strong super-shift with anti-YY1 in electrophoretic mobility shift assays using the *Tor1a* THABS and embryonic brain nuclear extract (data not shown).

In summary, we have identified THAP1 as an essential regulator of mESC potential, including viability and likely neuronal differentiation, the latter particularly for the naturally occurring C54Y mutation. These activities are likely due in part to direct regulation of gene expression but to a large extent to indirect regulation, the mechanisms of which are important to identify. Notably, dysregulated pathways in ESCs with mutations of THAP1 overlap with those seen in mouse models of DYT6, and the ESC system

Figure 7. Characterization of Neural Differentiation

(A) Schematic representation of cell-culture strategy of neural differentiation using protocol #1.

(B) Immunofluorescence analysis of Nestin (green; middle panel) and TuJ1 (red; right panel) of WT, *Thap1*$^{C54Y/C54Y}$ (KI), and *Thap1*$^{\Delta Exon2}$ (KO) differentiated cells at day 10 of differentiation. Bright field (left panel) and DAPI stain (blue) are shown. Scale bars, 100 μm.

(C) Bar graph depicting percentage of colonies with neuronal projection.

(D) qRT-PCR analysis of *Thap1*, pluripotent, and ectoderm marker genes during neural differentiation (protocol #1) of *Thap1*$^{C54Y/C54Y}$ (KI) and *Thap1*$^{\Delta Exon2}$ (KO) ESCs at the indicated time points. Data are presented relative to WT at day 0. The two-way ANOVA results for *Thap1*, pluripotent, and ectoderm marker genes during RA-induced differentiation can be found in Table S3. The Holm-Sidak multiple comparisons test was performed post hoc for each gene of interest by day, revealing significant differences between the genotypes. Data are presented as mean ± SEM of at least three independent experiments. *$p < 0.05$, ***$p < 0.005$, ****$p < 0.001$.

(E) Schema illustrating that THAP1 is required to silence the expression of the pluripotency factors and to activate the expression of the neural factors, as well as mediate ESC survival.

may potentially be exploited to discover how following differentiation, mutations of the ubiquitously expressed THAP1 protein can lead to a strictly neurologic disease.

EXPERIMENTAL PROCEDURES

Preparation of nuclear extracts and qRT-PCR gene expression analysis were performed as previously described (Ruiz et al., 2015).

Further experimental details and lists of antibodies, public datasets, and primer sets utilized in this study may be found in Supplemental Experimental Procedures and other Supplemental Information.

Cell Culture and EB Formation

Wild-type (WT), *Thap1*^{C54Y}, and *Thap1*$^{\Delta Exon2}$ ESCs were maintained on 0.1% gelatin-coated tissue culture plates on irradiated mouse embryonic fibroblasts (MEFs) in DMEM containing 15% FCS, 0.1 mM 2-mercaptoethanol, L-glutamine, non-essential amino acids, and LIF (1,000 units/mL) and penicillin-streptomycin (Thermo Fisher). Cells were passaged once onto gelatin-coated dishes and then aggregated to form EBs in 10-cm Petri dishes at 5×10^6/plate in the absence of LIF. Cells were harvested for extraction of total RNA at the indicated time points. All cell cultures were maintained at 37°C with 5% CO_2.

Differentiation Assays

Induction of neural differentiation was performed based on generation of EBs, using two different approaches (Okabe et al., 1996; Okada et al., 2004), with and without addition of RA as indicated in Supplemental Experimental Procedures.

Cellular Proliferation, Apoptosis Assay, and Cell-Cycle Analyses

Cellular proliferation, apoptosis assay, and cell-cycle analysis were performed using a Muse Cell Analyzer (Millipore) following the manufacturer's instructions.

Alkaline Phosphatase Activity

AP activity was measured using the Stemgent Alkaline Phosphatase Staining kit (Stemgent) following the manufacturer's recommendations.

Chromatin Immunoprecipitation with High-Throughput Sequencing

THAP1 ChIP-Seq was performed as described in Supplemental Experimental Procedures.

RNA-Seq and Analysis

RNA-Seq library preparation was performed at the Weill-Cornell Medical College Genomic Core Facility using the TrueSeq RNA sample preparation kit (Illumina RS-122-2001) and sequenced by the Illumina HiSeq 2,500 platform as 100-bp pair-ended reads.

Gene Ontology Analysis

For functional profiling of THAP1 binding regions identified by ChIP-Seq, GO analysis was performed using Panther software (http://pantherdb.org) (Mi et al., 2016). GO analysis from RNA-Seq datasets was performed using the web tool The Database for Annotation, Visualization and Integrated Discovery (DAVID) (http://david.abcc.ncifcrf.gov/) (Huang et al., 2009a, 2009b).

Statistical Analysis

All values are expressed as mean ± SD. Statistical analysis was performed by two-way ANOVA followed by Bonferroni's multiple testing corrections using GraphPad Prism 5 Software. A probability value of $p < 0.05$ was considered statistically significant.

ACCESSION NUMBERS

All next-generation sequencing data are deposited in NCBI GEO database under accession numbers GEO: GSE86947 and GSE86911.

SUPPLEMENTAL INFORMATION

Supplemental Information includes Supplemental Experimental Procedures, five figures, and four tables and can be found with this article online at http://dx.doi.org/10.1016/j.stemcr.2017.04.032.

AUTHOR CONTRIBUTIONS

Conceptualization, F.A., Z.Z., M.J.W., L.J.O., P.G.-A., T.P.Z., and M.E.E.; Methodology, K.K.; Formal analysis, F.A., Z.Z., R.S., C.W, and W.Z.; Investigation, F.A., Z.Z., K.N., R.W., M.H., and Y.S.; Writing – Original Draft, F.A. and M.E.E.; Writing – Review & Editing, Z.Z., P.G.-A., L.J.O., M.J.W., T.P.Z., and M.E.E.; Funding Acquisition, M.E.E.; Supervision and Project Administration, F.A. and M.E.E.

ACKNOWLEDGMENTS

We thank Dr. A. Alonso of the Weill-Cornell College of Medicine's Epigenomic Sequencing Core for expert advice for sequencing and library preparation. This work was funded by NIH R01NS081282 (to M.E.E. and L.J.O.) New York State Stem Cell Science (NYSTEM C029553 to M.E.E.), and the Huffington Foundation (T.P.Z.).

Received: October 11, 2016
Revised: April 26, 2017
Accepted: April 27, 2017
Published: June 1, 2017

REFERENCES

Aguilo, F., Zhang, F., Sancho, A., Fidalgo, M., Di Cecilia, S., Vashisht, A., Lee, D.-F., Chen, C.-H., Rengasamy, M., Andino, B., et al. (2015). Coordination of m(6)A mRNA methylation and gene transcription by ZFP217 regulates pluripotency and reprogramming. Cell Stem Cell *17*, 689–704.

Arnold, C.D., Gerlach, D., Stelzer, C., Boryń, Ł.M., Rath, M., and Stark, A. (2013). Genome-wide quantitative enhancer activity maps identified by STARR-seq. Science *339*, 1074–1077.

Ballas, N., Grunseich, C., Lu, D.D., Speh, J.C., and Mandel, G. (2005). REST and its corepressors mediate plasticity of neuronal gene chromatin throughout neurogenesis. Cell *121*, 645–657.

Bergsland, M., Ramsköld, D., Zaouter, C., Klum, S., Sandberg, R., and Muhr, J. (2011). Sequentially acting Sox transcription factors in neural lineage development. Genes Dev. *25*, 2453–2464.

Campagne, S., Muller, I., Milon, A., and Gervais, V. (2012). Towards the classification of DYT6 dystonia mutants in the DNA-binding domain of THAP1. Nucleic Acids Res. *40*, 9927–9940.

Cayrol, C., Lacroix, C., Mathe, C., Ecochard, V., Ceribelli, M., Loreau, E., Lazar, V., Dessen, P., Mantovani, R., Aguilar, L., et al. (2007). The THAP-zinc finger protein THAP1 regulates endothelial cell proliferation through modulation of pRB/E2F cell-cycle target genes. Blood *109*, 584–594.

Chen, Y., He, Z.X., Liu, A., Wang, K., Mao, W.W., Chu, J.X., Lu, Y., Fang, Z.F., Shi, Y.T., Yang, Q.Z., et al. (2003). Embryonic stem cells generated by nuclear transfer of human somatic nuclei into rabbit oocytes. Cell Res. *13*, 251–263.

Chipuk, J.E., and Green, D.R. (2005). Do inducers of apoptosis trigger caspase-independent cell death? Nat. Rev. Mol. Cell Biol. *6*, 268–275.

Clouaire, T., Roussigne, M., Ecochard, V., Mathe, C., Amalric, F., and Girard, J.-P. (2005). The THAP domain of THAP1 is a large C2CH module with zinc-dependent sequence-specific DNA-binding activity. Proc. Natl. Acad. Sci. USA *102*, 6907–6912.

Dejosez, M., Krumenacker, J.S., Zitur, L.J., Passeri, M., Chu, L.-F., Songyang, Z., Thomson, J.A., and Zwaka, T.P. (2008). Ronin is essential for embryogenesis and the pluripotency of mouse embryonic stem cells. Cell *133*, 1162–1174.

Erogullari, A., Hollstein, R., Seibler, P., Braunholz, D., Koschmidder, E., Depping, R., Eckhold, J., Lohnau, T., Gillessen-Kaesbach, G., Grünewald, A., et al. (2014). THAP1, the gene mutated in DYT6 dystonia, autoregulates its own expression. Biochim. Biophys. Acta *1839*, 1196–1204.

Fuchs, T., Gavarini, S., Saunders-Pullman, R., Raymond, D., Ehrlich, M.E., Bressman, S.B., and Ozelius, L.J. (2009). Mutations in the THAP1 gene are responsible for DYT6 primary torsion dystonia. Nat. Genet. *41*, 286–288.

Gavarini, S., Cayrol, C., Fuchs, T., Lyons, N., Ehrlich, M.E., Girard, J.-P., and Ozelius, L.J. (2010). Direct interaction between causative genes of DYT1 and DYT6 primary dystonia. Ann. Neurol. *68*, 549–553.

Gervais, V., Campagne, S., Durand, J., Muller, I., and Milon, A. (2013). NMR studies of a new family of DNA binding proteins: the THAP proteins. J. Biomol. NMR *56*, 3–15.

He, Y., and Casaccia-Bonnefil, P. (2008). The Yin and Yang of YY1 in the nervous system. J. Neurochem. *106*, 1493–1502.

Heintzman, N.D., Stuart, R.K., Hon, G., Fu, Y., Ching, C.W., Hawkins, R.D., Barrera, L.O., Van Calcar, S., Qu, C., Ching, K.A., et al. (2007). Distinct and predictive chromatin signatures of transcriptional promoters and enhancers in the human genome. Nat. Genet. *39*, 311–318.

Heintzman, N.D., Hon, G.C., Hawkins, R.D., Kheradpour, P., Stark, A., Harp, L.F., Ye, Z., Lee, L.K., Stuart, R.K., Ching, C.W., et al. (2009). Histone modifications at human enhancers reflect global cell-type-specific gene expression. Nature *459*, 108–112.

Höpfl, G., Gassmann, M., and Desbaillets, I. (2004). Differentiating embryonic stem cells into embryoid bodies. Methods Mol. Biol. *254*, 79–98.

Houlden, H., Schneider, S.A., Paudel, R., Melchers, A., Schwingenschuh, P., Edwards, M., Hardy, J., and Bhatia, K.P. (2010). THAP1 mutations (DYT6) are an additional cause of early-onset dystonia. Neurology *74*, 846–850.

Huang, D.W., Sherman, B.T., and Lempicki, R.A. (2009a). Systematic and integrative analysis of large gene lists using DAVID bioinformatics resources. Nat. Protoc. *4*, 44–57.

Huang, D.W., Sherman, B.T., and Lempicki, R.A. (2009b). Bioinformatics enrichment tools: paths toward the comprehensive functional analysis of large gene lists. Nucleic Acids Res. *37*, 1–13.

Kaiser, F.J., Osmanoric, A., Rakovic, A., Erogullari, A., Uflacker, N., Braunholz, D., Lohnau, T., Orolicki, S., Albrecht, M., Gillessen-Kaesbach, G., et al. (2010). The dystonia gene DYT1 is repressed by the transcription factor THAP1 (DYT6). Ann. Neurol. *68*, 554–559.

Kheradpour, P., and Kellis, M. (2014). Systematic discovery and characterization of regulatory motifs in ENCODE TF binding experiments. Nucleic Acids Res. *42*, 2976–2987.

Majumdar, S., and Rio, D.C. (2015). P transposable elements in Drosophila and other eukaryotic organisms. Microbiol. Spectr. *3*, MDNA3-0004-2014.

Mazars, R., Gonzalez-de-Peredo, A., Cayrol, C., Lavigne, A.-C., Vogel, J.L., Ortega, N., Lacroix, C., Gautier, V., Huet, G., Ray, A., et al. (2010). The THAP-zinc finger protein THAP1 associates with coactivator HCF-1 and O-GlcNAc transferase: a link between DYT6 and DYT3 dystonias. J. Biol. Chem. *285*, 13364–13371.

Mi, H., Poudel, S., Muruganujan, A., Casagrande, J.T., and Thomas, P.D. (2016). PANTHER version 10: expanded protein families and functions, and analysis tools. Nucleic Acids Res. *44*, D336–D342.

Okabe, S., Forsberg-Nilsson, K., Spiro, A.C., Segal, M., and McKay, R.D. (1996). Development of neuronal precursor cells and functional postmitotic neurons from embryonic stem cells in vitro. Mech. Dev. *59*, 89–102.

Okada, Y., Shimazaki, T., Sobue, G., and Okano, H. (2004). Retinoic-acid-concentration-dependent acquisition of neural cell identity during in vitro differentiation of mouse embryonic stem cells. Dev. Biol. *275*, 124–142.

Ortiz-Virumbrales, M., Ruiz, M., Hone, E., Dolios, G., Wang, R., Morant, A., Kottwitz, J., Ozelius, L.J., Gandy, S., and Ehrlich, M.E. (2014). Dystonia type 6 gene product Thap1: identification of a 50 kDa DNA-binding species in neuronal nuclear fractions. Acta Neuropathol. Commun. *2*, 139.

Palmqvist, L., Glover, C.H., Hsu, L., Lu, M., Bossen, B., Piret, J.M., Humphries, R.K., and Helgason, C.D. (2005). Correlation of murine embryonic stem cell gene expression profiles with functional measures of pluripotency. Stem Cells *23*, 663–680.

Rada-Iglesias, A., Bajpai, R., Swigut, T., Brugmann, S.A., Flynn, R.A., and Wysocka, J. (2011). A unique chromatin signature uncovers early developmental enhancers in humans. Nature *470*, 279–283.

Roussigne, M., Cayrol, C., Clouaire, T., Amalric, F., and Girard, J.-P. (2003). THAP1 is a nuclear proapoptotic factor that links prostate-apoptosis-response-4 (Par-4) to PML nuclear bodies. Oncogene *22*, 2432–2442.

Ruiz, M., Perez-Garcia, G., Ortiz-Virumbrales, M., Méneret, A., Morant, A., Kottwitz, J., Fuchs, T., Bonet, J., Gonzalez-Alegre, P., Hof, P.R., et al. (2015). Abnormalities of motor function, transcription and cerebellar structure in mouse models of THAP1 dystonia. Hum. Mol. Genet. *24*, 7159–7170.

Savarese, F., Dávila, A., Nechanitzky, R., De La Rosa-Velazquez, I., Pereira, C.F., Engelke, R., Takahashi, K., Jenuwein, T., Kohwi-Shigematsu, T., Fisher, A.G., et al. (2009). Satb1 and Satb2 regulate embryonic stem cell differentiation and Nanog expression. Genes Dev. *23*, 2625–2638.

Schneider, S.A., Ramirez, A., Shafiee, K., Kaiser, F.J., Erogullari, A., Brüggemann, N., Winkler, S., Bahman, I., Osmanovic, A., Shafa, M.A., et al. (2011). Homozygous THAP1 mutations as cause of early-onset generalized dystonia. Mov. Disord. *26*, 858–861.

Sengel, C., Gavarini, S., Sharma, N., Ozelius, L.J., and Bragg, D.C. (2011). Dimerization of the DYT6 dystonia protein, THAP1, requires residues within the coiled-coil domain. J. Neurochem. *118*, 1087–1100.

Vemula, S.R., Xiao, J., Zhao, Y., Bastian, R.W., Perlmutter, J.S., Racette, B.A., Paniello, R.C., Wszolek, Z.K., Uitti, R.J., Van Gerpen, J.A., et al. (2014). A rare sequence variant in intron 1 of THAP1 is associated with primary dystonia. Mol. Genet. Genomic Med. *2*, 261–272.

Visel, A., Blow, M.J., Li, Z., Zhang, T., Akiyama, J.A., Holt, A., Plajzer-Frick, I., Shoukry, M., Wright, C., Chen, F., et al. (2009). ChIP-seq accurately predicts tissue-specific activity of enhancers. Nature *457*, 854–858.

Xiromerisiou, G., Houlden, H., Scarmeas, N., Stamelou, M., Kara, E., Hardy, J., Lees, A.J., Korlipara, P., Limousin, P., Paudel, R., et al. (2012). THAP1 mutations and dystonia phenotypes: genotype phenotype correlations. Mov. Disord. *27*, 1290–1294.

Youle, R.J., and Strasser, A. (2008). The BCL-2 protein family: opposing activities that mediate cell death. Nat. Rev. Mol. Cell Biol. *9*, 47–59.

Stem Cell Reports, Volume *9*

Supplemental Information

THAP1: Role in Mouse Embryonic Stem Cell Survival and Differentiation

Francesca Aguilo, Zuchra Zakirova, Katie Nolan, Ryan Wagner, Rajal Sharma, Megan Hogan, Chengguo Wei, Yifei Sun, Martin J. Walsh, Kevin Kelley, Weijia Zhang, Laurie J. Ozelius, Pedro Gonzalez-Alegre, Thomas P. Zwaka, and Michelle E. Ehrlich

FIGURE S1, related to FIGURE 3

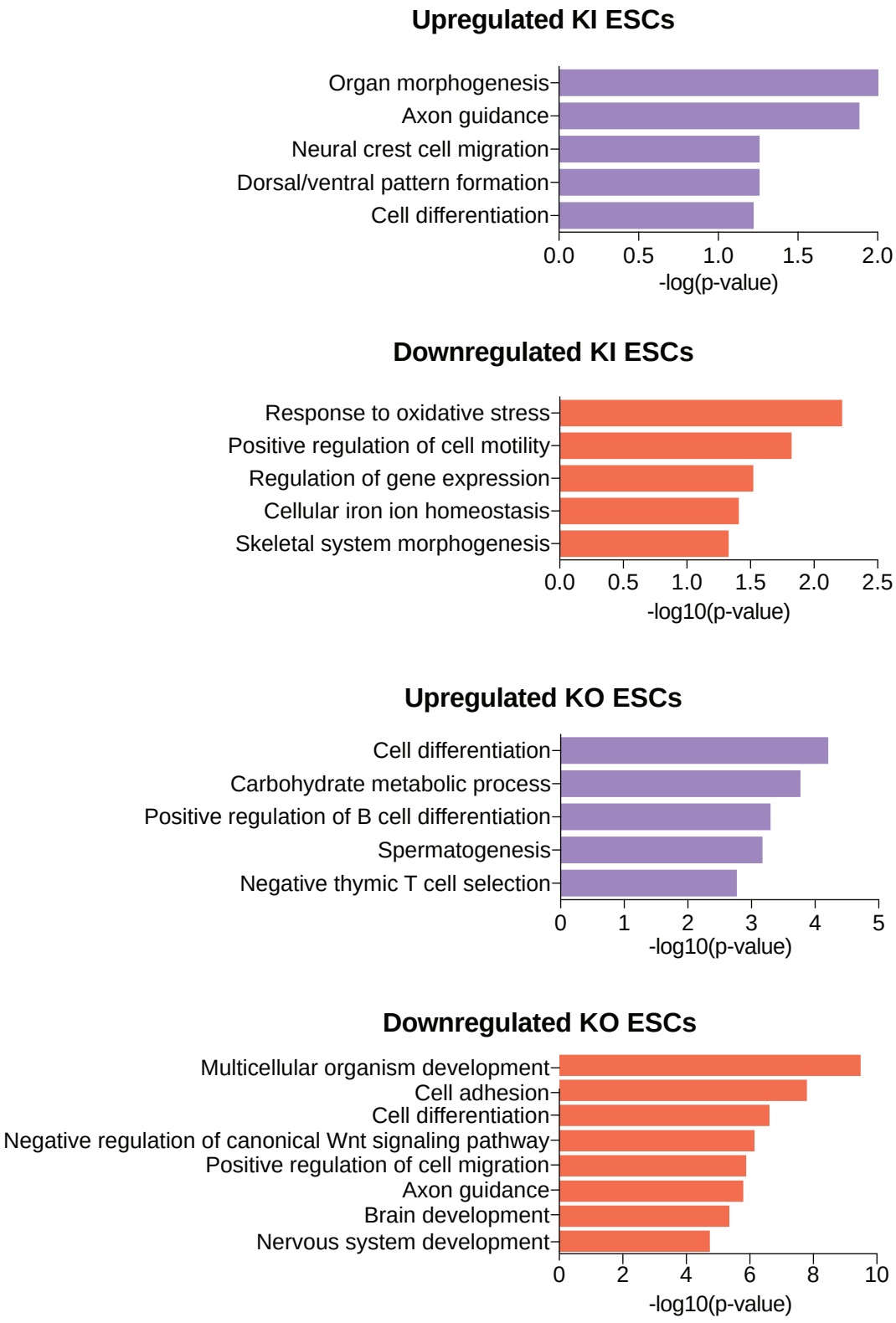

FIGURE S2, related to FIGURE 4

A

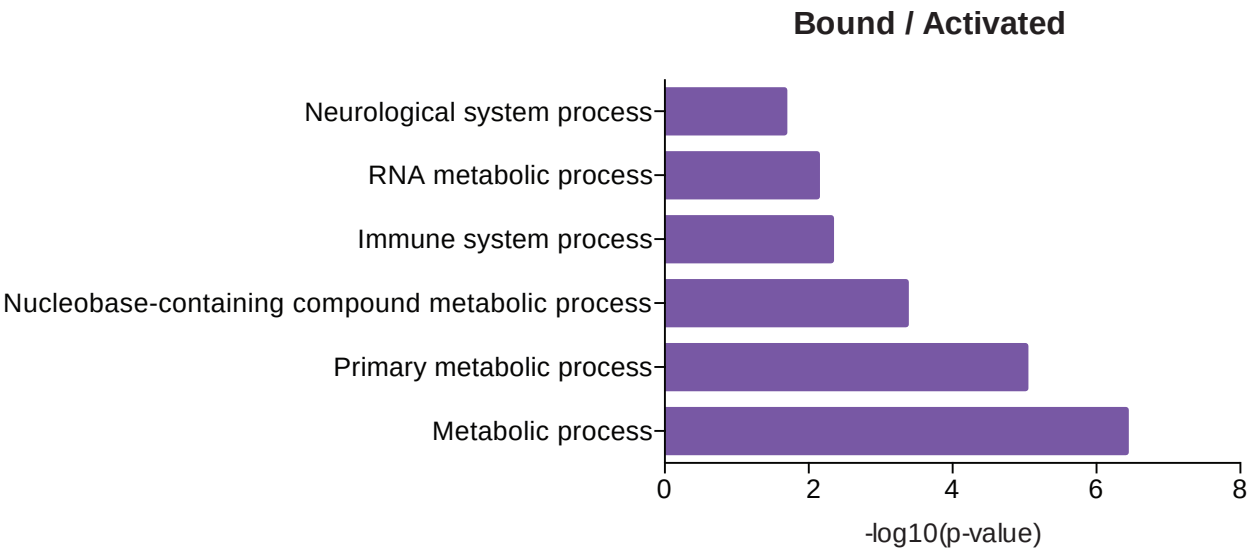

B

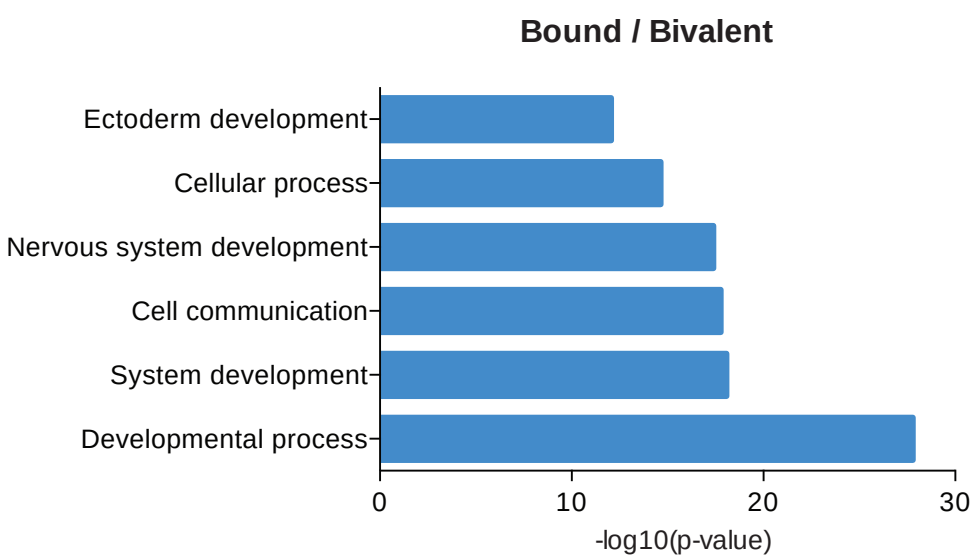

C

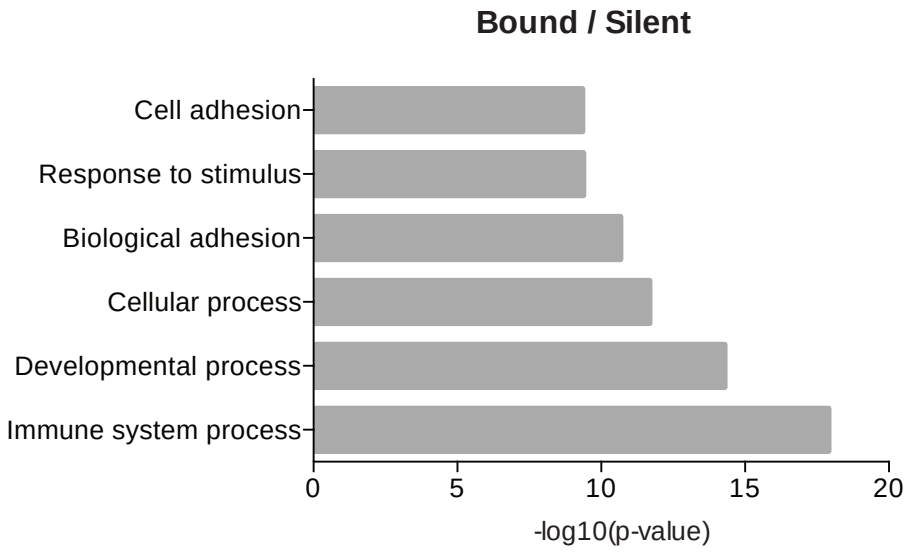

FIGURE S3, related to FIGURE 6

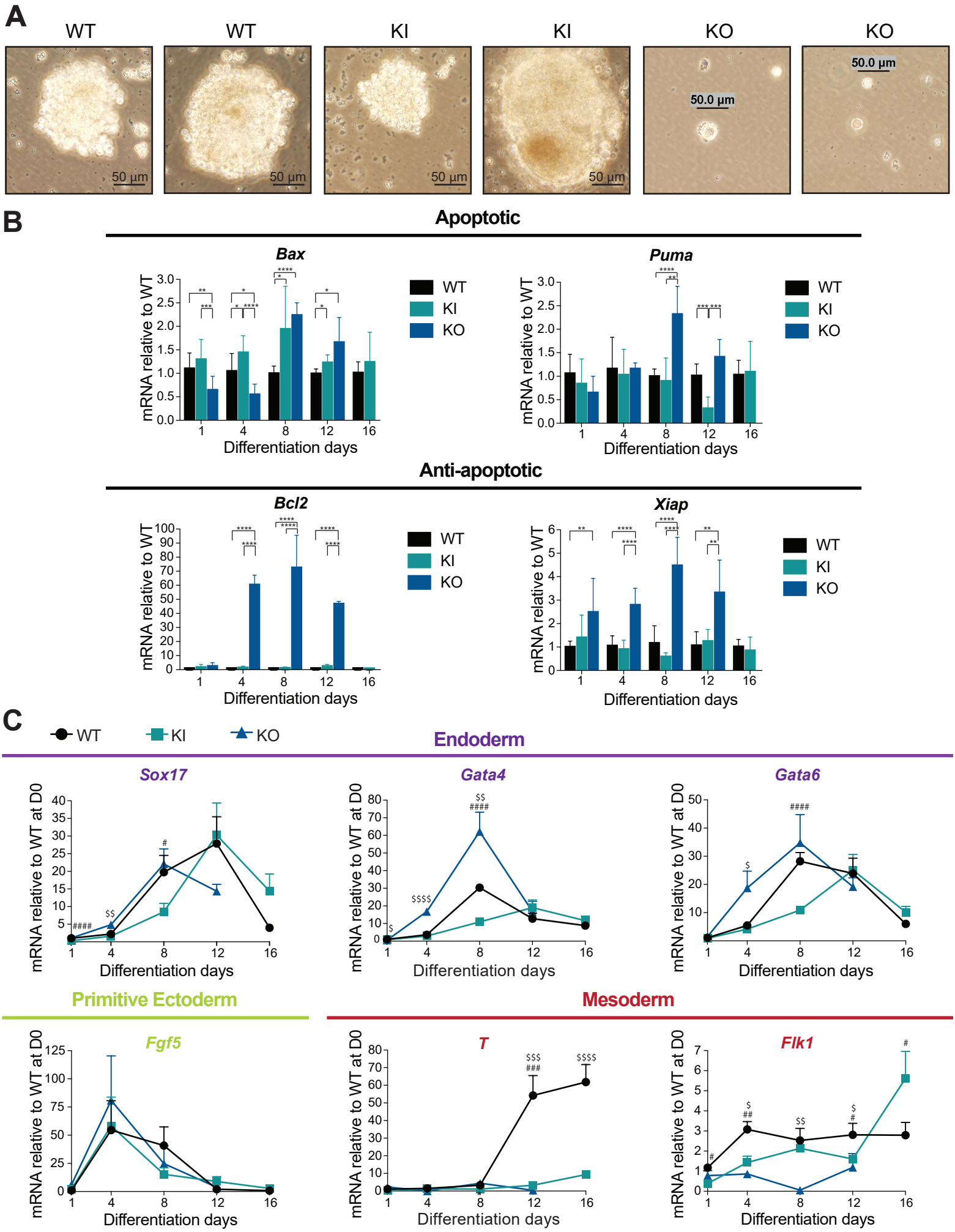

FIGURE S4, related to FIGURE 6

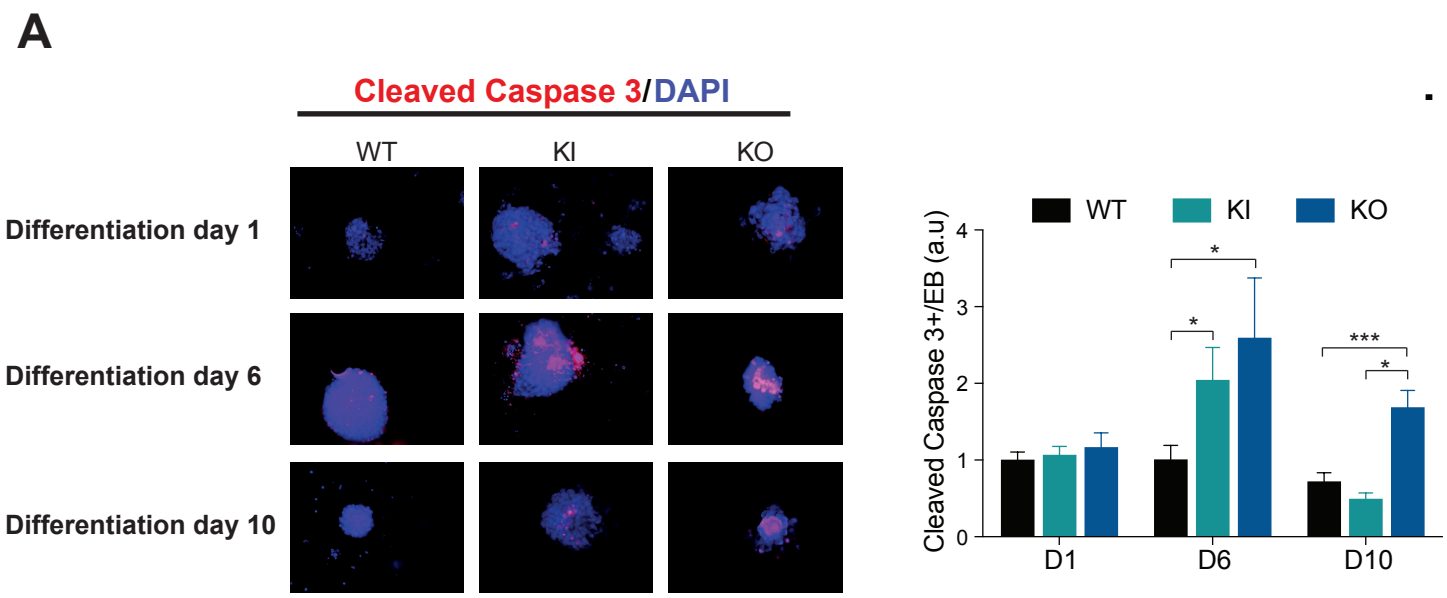

FIGURE S5, related to FIGURE 7

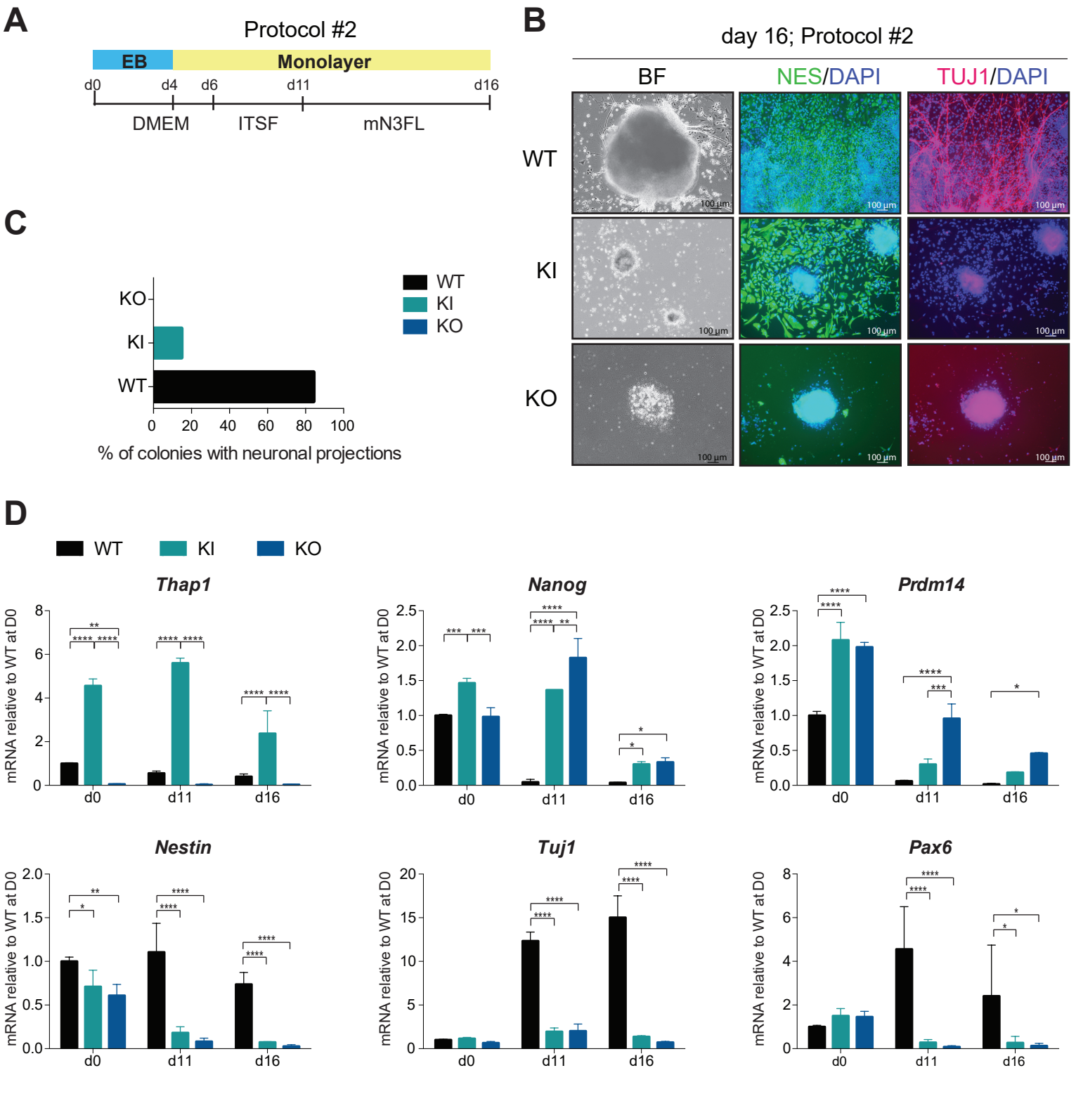

SUPPLEMENTAL FIGURE LEGENDS

Figure S1, related to Figure 3. Gene ontology analysis of uniquely regulated genes.

Gene ontology (GO) analyses of biological processes of uniquely upregulated and downregulated genes in *Thap1*$^{C54Y/C54Y}$ (KI) and *Thap1*$^{\Delta Exon2}$ (KO) ESCs from the RNA-Seq datasets. The p-value for the enrichment of biological process GO-term is shown.

Figure S2, related to Figure 4. Gene ontology analysis of THAP1 bound genes.

Gene ontology (GO) analyses of biological processes of THAP1 bound and activated genes (A), THAP1 bound and bivalent genes (B), and THAP1 bound and silent genes (C) as described under the methods section. The p-value for the enrichment of biological process GO-term is shown.

Figure S3, related to Figure 6. THAP1 is required for normal embryoid body formation.

(A) Bright field showing WT, *Thap1*$^{C54Y/C54Y}$ (KI) and *Thap1*$^{\Delta Exon2}$ (KO) EB morphology. The scale bar represents 50μm.

(B) RT-qPCR analysis of pro-apoptotic genes (*Bax* and *Puma*) and anti-apoptotic genes (*Bcl2* and *Xiap)* during EB differentiation of WT, *Thap1*$^{C54Y/C54Y}$ (KI) and *Thap1*$^{\Delta Exon2}$ (KO) ESCs at the indicated time points. Data are normalized to WT, relative for each day of differentiation. Significant differences were observed by two-way ANOVA among the genotypes when examining expression of *Bax* [F (2,63) = 7.609, p= 0.0011], *Puma* [F (2, 85) = 1481, p = 0.0009], *Bcl2* [F (2,9) = 74.64, p < 0.0001] and *Xiap* [F (2, 67) = 54.39, p < 0.0001]. Bonferroni multiple comparisons test was performed *post hoc* revealing significant differences between the genotypes. Data are represented as mean ± SEM of three independent experiments. *p < 0.05; **p < 0.01, ***p < 0.005, ****p < 0.001.

(C) RT-qPCR analysis of endodermal (*Sox17*, *Gata4* and *Gata6*), mesodermal (*T* and *Flk1*) and primitive ectodermal markers (*Fgf5*) during EB differentiation of WT, *Thap1*$^{C54Y/C54Y}$ (KI) and *Thap1*$^{\Delta Exon2}$ (KO) ESCs at the indicated time points. Data are normalized to WT, relative to D0. The two-way ANOVA results can be found in Table S3. Bonferroni multiple comparisons test was performed *post hoc* revealing significant differences between the genotypes. Data are represented as mean ± SEM of three independent experiments. *p < 0.05; **p < 0.01, ***p < 0.005, ****p < 0.001 relative to WT. Symbol '#' denotes differences between KI vs WT, and symbol '$' denotes differences between KO vs WT.

Figure S4, related to Figure 6. THAP1 is required for ES cell survival

(A) Wild-type (WT), *Thap1*$^{C54Y/C54Y}$ (KI) and *Thap1*$^{\Delta Exon2}$ (KO) EBs were immunostained for cleaved caspase-3 (CC3) on differentiation days 1, 6 and 10. Quantification of CC3+ immunopositive EBs (right panel) was performed by scoring CC3+ immunopositive cells as a function of total EB area, normalized to WT for each differentiation day. Two-way ANOVA was performed, followed by Bonferroni post testing corrections. Data are represented as mean ± SEM; n = 10 per group for each day, data pooled from three independent experiments. *p < 0.05; **p < 0.01, *** p < 0.005, ****p < 0.001.

(B) The pan caspase inhibitor, Z-VAD-FMK does not inhibit cell death in *Thap1*$^{C54Y/C54Y}$ (KI) and *Thap1*$^{\Delta Exon2}$ (KO) EBs over four days of EB differentiation. Two-way ANOVA was performed for each day of treatment, followed by Bonferroni post testing corrections. Data are represented as mean ± SEM of three independent experiments. *p < 0.05; **p < 0.01, ***p < 0.005, ****p < 0.001.

Figure S5, related to Figure 7. Characterization of neural differentiation cell cultures

(A) Schematic diagram of Protocol #2 for neural differentiation.

(B) Immunofluorescence analysis of NESTIN (green; middle panel) and TUJ1 (red; right panel) of WT, *Thap1*$^{C54Y/C54Y}$ (KI) and *Thap1*$^{\Delta Exon2}$ (KO) differentiated cells at the indicated day using protocol #2. Bright field (left panel) and DAPI stain (blue) are shown. The scale bar represents 100 μm.

(C) Bar graph depicting % of colonies with neuronal projection.

(D) RT-qPCR analysis of *Thap1*, pluripotency markers (*Nanog* and *Prdm14*), and ectoderm marker genes (*Nestin*, *Tuj1*, and *Pax6*) during neural differentiation of WT, *Thap1*$^{C54Y/C54Y}$ (KI) and *Thap1*$^{\Delta Exon2}$ (KO) ESCs at the indicated time points. Data are represented relative to WT at day 0. Two-way RM ANOVA was performed for *Thap1*, revealing an interaction effect [F (4,27) = 24.72, p < 0.0001], in addition, significant differences were observed by days [F (2,27) = 31.16, p < 0.0001], and by genotype [F (2,27) = 430.7, p < 0.0001]. Two-way RM ANOVA was performed for *Nanog*, revealing an interaction effect [F (4,16) = 55.52, p < 0.0001], in addition, significant differences were observed by days [F (2,16) = 171.5, p < 0.0001], and by genotype [F (2,16) = 99.32, p < 0.0001]. Two-way RM ANOVA was performed for *Prdm14*, revealing an interaction effect [F (4,9) = 11.84, p = 0.0012], in addition, significant differences were observed by days [F (2,9) = 275.1, p < 0.0001], and by genotype [F (2,9) = 67.04, p < 0.0001]. Two-way RM ANOVA was performed for *Nestin*, revealing an interaction effect [F (4,27) = 6.423, p = 0.0009], in addition, significant differences were observed by days [F (2,27) = 35.89, p < 0.0001], and by genotype [F (2,27) = 85.86, p < 0.0001]. Two-way RM ANOVA was performed for *Tuj1*, revealing an interaction effect [F (4,27) = 76.88, p < 0.0001], significant differences were observed by days [F (2,27) = 95.69, p < 0.0001], and by genotype [F (2,27) = 294.6, p < 0.0001]. Two-way RM ANOVA was performed for *Pax6*, revealing an interaction effect [F (4,26) = 7.176, p = 0.0005], significant differences were observed by genotype [F (2,26) = 14.86, p < 0.0001], but not

by day. Holm-Sidak's multiple comparisons test was performed *post hoc* revealing significant differences between the genotypes. Data are represented as mean ± SEM of at least three independent experiments. *p < 0.05; **p < 0.01, ***p < 0.005, ****p < 0.001.

SUPPLEMENTAL TABLES

Table S1, related to Figure 3: RNA-Seq. Gene expression in KI and KO ESCs compared to WT ESCs. Uniquely regulated genes are also depicted. Fold-change is shown. See separate excel File, Table S1.xlsx

Table S2, related to Figure 4: ChIP-Seq for THAP1 in WT ESCs. See separate excel File, Table S2.xlsx

Table S3, related to Figure 6, Figure 7 and Figure S3: Statistical analyses tables for the indicated figures. See separate excel File, Table S3.xlsx

Table S4, related to experimental procedures: RT-qPCR primers used for gene expression analysis and ChIP validation. Primers used for ESCs and mice genotyping. See separate excel File, Table S4.xlsx

SUPPLEMENTAL EXPERIMENTAL PROCEDURES

Antibodies

The following commercially available antibodies were used at the indicated concentrations for western blot: anti-THAP1 (Proteintech, 12584-1-AP, 1:1000), anti-HDAC1 (Abcam, ab7028, 1:1000), and anti-PGK1/2 (SantaCruz, sc-23805, 1:1000). ChIP analysis was performed with the indicated amount of anti-THAP1 antibody and number of cells: (Proteintech, 12584-1-AP; 5 μg antibody for 1 x 10^7 cells). For immunocytochemistry (ICC) analysis SSEA1 (BD Pharmigen, 561560, 1:400), anti-OCT4 (Abcam, ab19857, 1:1000), anti-NESTIN (NovusBio, NB100-1604, 1:1000), anti-β3 Tubulin antibody (TUJ-1) (SantaCruz, sc-58888, 1:250) and anti-cleaved caspase 3 (CC3) (CellSignaling, 9661, 1:400) were used. All cells were counterstained with diamidino-2-phenylindole (DAPI) solution (ThermoFisher, 62248, 1:1000).

Derivation of mouse ESCs

Animal use was approved by the IACUC committee at the Icahn School of Medicine at Mount Sinai. Heterozygous *THAP1*^{C54Y} female mice were super-ovulated by intraperitoneal injection of 5 IU pregnant mare's serum (PMS; National Hormone and Peptide Program) followed 48 hours later by 5 IU of human chorionic gonadotropin (HCG; National Hormone and Peptide *THAP1*^{C54Y} male mice (1 female per male). Three days later, 8-cell stage embryos were isolated from the oviduct and uterus of the females using FHM media (Millipore Specialty Media, MR-024-D), and cultured overnight in KSOM + amino acids media (Millipore Specialty Media, MR-121-D). The next day, 24 blastocysts were plated onto irradiated mouse embryo fibroblasts in a gelatin-coated 24-well plate (one blastocyst per well), and cultured in a 6% CO2 incubator undisturbed for 4 days. All culture steps were performed using ES media with LIF (see below).

Outgrowths that were visible after 4 days of culture were isolated using a micropipettor, and transferred to a small volume of 0.25% trypsin, 2.21 mM EDTA (Corning, 25-053-Cl). After disruption of the outgrowth, the cells were re-plated into 24-well plates with irradiated mouse embryonic fibroblasts. Cell growth was monitored, and clones that contained colonies with ES-like morphology were passaged through 6-well plates to 60 mm dishes. DNA samples were prepared from parallel cultures that were used for genotyping of the resulting ES clones. Of the 24 plated blastocysts, 6 ES clones were derived. Genotyping revealed that clones 5, 14 and 18 were wild-type, clone 9 was heterozygous for *THAP1*^{C54Y}, and clones 6 and 17 were homozygous for *THAP1*^{C54Y}.

For generation of *Thap1*$^{\Delta Exon2}$ ESCs, cre-mediated excision of exon 2 was performed by transfection of 1.5 x 10^6 *Thap1*$^{C54Y/C54Y}$ ESCs with pSalk-Cre (pTZ1111), a mammalian expression vector in which pCMV promoter drives Cre recombinase expression as previously described (Dejosez et al., 2008).

Differentiation assays

Induction of neural differentiation was performed based on generation of EBs, using two different approaches, with and without addition of RA. Protocol #1 was adapted from (Okada et al., 2004). Two-day-old EBs were cultured in N2B27 medium [DMEM/F-12, 0.1 mM 2-mercaptoethanol, N2 supplement (100X) (ThermoFisher), B27 supplement (50X) (ThermoFisher)], and penicillin/streptomycin (ThermoFisher) supplemented with 1 μM RA (Sigma-Aldrich) for 4 days. At day 6, EBs were plated in tissue culture dishes pre-coated with 0.1% gelatin and propagated in the same medium for additional 4 days. Medium was replenished every 2 days. Protocol #2 was adapted from (Okabe et al., 1996) with some modifications. Four-day-old EBs were plated in tissue culture dishes pre-coated with 0.1% gelatin and propagated for 7 days in ITSFn medium [DMEM/F-12 (Dulbecco's Modified Eagle Medium/Nutrient Mixture F-12)] containing insulin (5 μg/mL), transferrin (50 μg/mL), 30 nM selenium chloride, and fibronectin (5 μg/mL). At day 11, cells were cultured in mN3FL medium [DMEM/F12 supplemented with insulin (25 μg/mL), transferrin (50 μg/mL), progesterone (20 nM), putrescine (100 μM), selenium chloride (30 nM), bFGF (5 ng/mL), and laminin (1 μg/mL)] for an additional 5 days. Cells were harvested for extraction of total RNA and ICC at the indicated time points.

Immunofluorescence staining

Cells were fixed in 4% paraformaldehyde (PFA) at room temperature (RT) for 20 min and then permeabilized at room temperature (RT) for 30 min with 0.25% Triton-X-100 in TBS. Cells were then washed twice with PBS and blocking was performed for 30 min with 3% goat serum in TBS. The cells were stained with the specified antibodies overnight at 4°C in 1% goat serum in TBS. After overnight incubation, the cover slips were washed thoroughly with TBS and incubated in either goat anti-rabbit IgG H&L (Alexa Fluor® 488, ab150077, 1:400), goat anti-mouse IgG H&L (Alexa Fluor® 594, ab150116, 1:400) or goat anti-chicken IgY H&L (Alexa Fluor® 488, ab150169, 1:400) secondary antibody (Abcam) for one hour. For nuclear staining, 4', 6-diamidino-2-phenylindole (DAPI Solution (1 mg/mL) diluted 1:1000 in DPBS) was added to each well and incubated for 10 minutes, after which the fixed cells were again washed with TBS three times. Cells were examined under an Olympus IX51 inverted fluorescent microscope.

Terminal deoxynucleotidyl transferase dUTP nick end labeling (TUNEL) immunocytochemistry

On differentiation days 1, 6 and 10 embryoid bodies (EBs) were fixed with 4% paraformaldehyde (PFA). EBs were assayed with Roche *In Situ* Cell Death Detection Kit (Catalog No. 11684795910; Sigma-Aldridge) per manufacturer's instructions followed by nuclear counterstaining using 4', 6-diamidino-2-phenylindole (DAPI Solution (Catalog No. 62248, ThermoFisher Scientific). EBs were examined under an Olympus BX61 fluorescent microscope. For quantification of TUNEL + immunopositive EBs, a minimum of ten high-power fields from each genotype per day were chosen and quantified using a CellProfiler (Carpenter et al., 2006; Kamentsky et al., 2011) pipeline which scored TUNEL immunopositive cells as a function of total EB area.

Cell proliferation assay with Z-VAD-FMK

Cell viability was assessed on the first day of EB differentiation with and without Z-VAD-FMK pan caspase inhibitor (Selleckchem) as previously described (Lubitz et al., 2007). Briefly, mass culture of EBs was started with 1.2×10^6 ES cells per bacterial dish by using standard EB medium without LIF. Resulting EBs were grown in the presence of 40 μM Z-VAD-FMK prepared in dimethyl sulfoxide (DMSO) or the same vol/vol pure DMSO and percentage of cell viability was assessed on four consecutive days (in triplicates) using Muse™ Cell Analyzer (Millipore; Billerica, MA) following the manufacturer's instructions. Z-VAD-FMK was replenished daily. Experiment was performed in quadruplicate.

Preparation of nuclear extracts

Cells were expanded in 100 mm diameter tissue culture plates, washed with cold PBS, and scraped off, followed by nuclear extract preparation as previously described with some modifications (Dignam et al., 1983). Briefly, the cellular pellet was resuspended in at least 5 volumes of buffer A (10 mM HEPES pH 7.9, 1.5 mM $MgCl_2$, 10 mM KCl, 1 mM DTT) in the presence of protease inhibitors (3 μg/ml aprotinin, 750 μg/ml benzamidine, 1 mM phenylmethylsulfonyl fluoride, 5 mM NaF and 2 mM sodium orthovanadate) and incubated for 10 minutes in ice. Following centrifugation, the pellet was resuspended in 2 volumes of buffer A, homogenized with a Dounce homogenizer, and spun down at maximum speed for 5 minutes. Nuclei were then resuspended in 2 volumes of buffer B (20 mM HEPES pH 7.9, 1.5 mM $MgCl_2$, 500 mM NaCl, 25% Glycerol, 0.5 mM EDTA, 1 mM DTT) supplemented with protease inhibitors and incubated in a rotator at 4 degrees for 30 minutes. The resulting samples were spun down at maximum speed for 15 minutes and frozen at -80 ^oC for further analysis.

RT-qPCR analysis

Total RNA purification was performed with the miRNeasy mini kit (Qiagen), and was carried out according to the manufacturer's instructions. Five hundred nanograms of RNA were reversed-transcribed using the High Capacity RNA-to-cDNA Kit (Applied Biosystems, Foster City, CA, USA). The cDNA solution was subjected to real-time qPCR in a Step-One Plus system (Applied Biosystems) using the PerfeCTa SYBR Green FastMix ROX (Quanta BioSciences). Quantitative PCR consisted of 40 cycles, 15 s at 95 °C and 30 s at 60 °C each, followed by dissociation curve analysis. Gene expression specific primers used for this study are listed in **Table S4**. *β-actin* mRNA was assayed as loading control.

Chromatin immunoprecipitation with high-throughput sequencing (ChIP-Seq)

THAP1 ChIP-Seq was carried out using methods described in (Hnisz et al., 2016). THAP1 mouse embryonic stem cells (500 million cells) were dual-crosslinked at room temperature with 1.5 mM ethylene glycol bis (sulfosuccinimidyl succinate) (EGS) for 30 minutes, followed by 1% formaldehyde for 10 min, and then neutralized with 125 mM glycine. Crosslinked cells were washed three times with ice-cold PBS, snap-frozen in liquid nitrogen, and stored at -80°C before further processing. 250 μl of Protein G Dynabeads (Life Technologies) were blocked with 0.5% BSA (w/v) in PBS, and pre-incubated with 25 μg of anti-THAP1 antibody (validated for ChIP in Gavarini et al., 2010). Nuclei were isolated as previously described (Lee et al., 2006), and sonicated in lysis buffer (20 mM Tris-HCl pH 8.0, 150 mM NaCl, 2 mM EDTA pH 8.0, 0.1% SDS, and 1% Triton X-100) on a Fisher Sonic Dismembrator for 14 cycles at 30s each on ice (power 5) with 60 s between cycles. Sonicated lysates were cleared once by centrifugation and incubated overnight at 4°C with magnetic beads bound with antibody. Protein-DNA complexes were sequentially washed with buffer A (50 mM HEPES-KOH pH7.9, 140 mM NaCl, 1 mM EDTA pH 8.0, 0.1% Na-Deoxycholate, 1% Triton X-100, 0.1% SDS), buffer B (50 mM HEPES-KOH pH7.9, 500 mM NaCl, 1 mM EDTA pH 8.0, 0.1% Na-Deoxycholate, 1% Triton X-100,

0.1% SDS), buffer C (20 mM Tris-HCl pH8.0, 250 mM LiCl, 1mM EDTA pH 8.0, 0.5% Na-Deoxycholate, 0.5% IGEPAL C-630 0.1% SDS) and buffer D (TE with 50 mM NaCl).

Library preparation

ChIP-Seq libraries were prepared using an adaptation of the Nextera Library Preparation protocol (Illumina), as described in (Hnisz et al., 2016). ChIP DNA fragments were end-repaired using T4 DNA polymerase (NEB) followed by A-tailing with Klenow (NEB). A biotinylated bridge linker (F: /5Phos/CGCGATATC/iBiodT/TATCTGACT; R: /5Phos/GTCAGATAAGATATCGCGT) with T- overhangs was added and the proximity ligation was performed overnight at 16°C in 1.5 mL volume. Un-ligated DNA was digested with exonuclease and lambda nuclease (NEB). DNA was eluted off the beads in elution buffer (50 mM Tris-HCL pH 8.0, 10 mM EDTA, 1% SDS) followed by overnight crosslink reversal, RNAse A treatment, and proteinase K digestion. A phenol:chloroform:isoamyl alcohol extraction was performed followed by an ethanol precipitation. Precipitated DNA was resuspended in Nextera DNA resuspension buffer (Illumina). The DNA was then tagmented with the Nextera Tagmentation kit (Illumina). The tagmented library was purified with a Zymo column and was bound to Streptavidin beads to enrich for ligation junctions (containing the biotinylated bridge linker). 15 cycles of the polymerase chain reaction were performed to amplify the library. The amplified library was size selected (200-500 bp) with a Pippin prep machine and sequenced with 100x100 paired-end sequencing on an Illumina Hi-Seq 2500 platform.

ChIP-Seq analysis

All ChIP-Seq datasets were processed with custom script ("Dowen et al. pipeline") as previously described (Dowen et al., 2014; Hnisz et al., 2016). Image analysis and base calling was done using the Solexa pipeline. Reads were examined for the presence of at least 10 base pairs of linker sequence. Reads that did not contain linker were not processed further. Reads containing linker were trimmed using cutadapt (cutadapt -m 17 –a forward=ACGCGATATCTTATCTGACT –a reverse=AGTCAGATAAGATATCGCGT -- overlap 10) (http://code.google.com/p/cutadapt/). Trimmed mate pairs were mapped independently to mm9 using Bowtie version 1.1.1 (bowtie -e 70 -k 1 -m 1 -v 2 -p 4 --best --strata --S) (Langmead et al., 2009). To remove PCR bias artifacts, reads were filtered for redundancy: PETs with identical genomic coordinates and strand information at both ends were collapsed into a single PET. Regions of local enrichment (PET peaks) were called using MACS 1.4.2 (Zhang et al., 2008) with the parameters "-p 1e-09-no-lambda –no-model", and an FDR of 0.01. Genes within 1 Kb of THAP1 peaks were identified using BETA-minus (Wang et al., 2013).

ChIP-Seq signal tracks were presented by Integrative Genomics Viewer (IGV) software (http://www.broadinstitute.org/igv/). THAP1 *de-novo* motif analysis and transcription factor binding sequence motifs enriched in THAP1 peak sequences were obtained with MEME-ChIP software (http://meme.nbcr.net/meme/cgi-bin/meme-chip.cgi) (Machanick and Bailey, 2011).

To examine chromatin patterns, enrichment profiles around THAP1 binding peaks with previously reported ESC ChIP-Seq datasets were generated. Each gene in the mouse genome was also classified into (i) active, containing H3K4me3 at the TSS and di-methylated histone H3 Lys 79 (H3K79me2) within the first 5 Kb of the gene body; (ii) bivalent or poised, associated with H3K4me3 and H3K27me3 at the TSS and (iii) silent, associated with the absence of H3K4me3 and H3K79me2 and the possibility to contain H3K27me3, and overlapped the THAP1-bound peaks. Below is the list of ChIP-Seq datasets used, corresponding GEO Accession numbers and publication:

Datasets	GEO Accession Number	Publication
p300	GSM918750	(Consortium, 2012; Yue et al., 2014)
MED1	GSM560347, GSM560348	(Kagey et al., 2010)
H3K4me1	GSM769009	(Yue et al., 2014)
H3K27ac	GSM594578, GSM594579	(Creyghton et al., 2010)
Pol2 Ser-5	GSM515662	(Rahl et al., 2010)
H3K4me3	GSM769008, GSE11724	(Marson et al., 2008; Yue et al., 2014)
H3K79me2	GSE11724	(Marson et al., 2008)
H3K27me3	GSM1000089, GSM307619	(Mikkelsen et al., 2007; Yue et al., 2014)

ChIP qRT-PCR validation

ChIP experiments were performed as described (Aguilo et al., 2016). Fold enrichment over 10% input was calculated using the 2DeltaCt method. The primer sets used for ChIP analysis are listed in **Table S4**.

RNA-Seq library preparation

RNA-Seq library preparation was performed at the Weill Cornell Medical College Genomic Core facility (New York) using the TrueSeq RNA sample preparation kit (Illumina RS-122-2001) as per manufacturer's recommendations. Samples were sequenced by the Illumina HiSeq 2500 platform (Illumina) as 100 bp pair-ended reads.

RNA-Seq analysis

RNA-Seq reads were filtered and trimmed using Trimmomatic (Bolger et al., 2014) and then aligned to the mm9 mouse reference genome and indexes based on UCSC annotations using TopHat (Trapnell et al., 2009). HT-seq (Anders et al., 2015) was used to find the read counts across the UCSC reference genome. Differentially expressed genes were identified by the R package DESeq2 (Love et al., 2014) using a false discovery rate (FDR) < 0.1 and fold-change >1.5.

Heat maps

Heat maps were derived using counts transformed by the varianceStabilizingTransformation function in DESeq2. Counts were then normalized by Z-score across samples and plotted.

SUPPLEMENTAL REFERENCES

Aguilo, F., Li, S., Balasubramaniyan, N., Sancho, A., Benko, S., Zhang, F., Vashisht, A., Rengasamy, M., Andino, B., Chen, C.H., *et al.* (2016). Deposition of 5-Methylcytosine on Enhancer RNAs Enables the Coactivator Function of PGC-1alpha. Cell Rep *14*, 479-492.

Anders, S., Pyl, P.T., and Huber, W. (2015). HTSeq--a Python framework to work with high-throughput sequencing data. Bioinformatics *31*, 166-169.

Bolger, A.M., Lohse, M., and Usadel, B. (2014). Trimmomatic: a flexible trimmer for Illumina sequence data. Bioinformatics *30*, 2114-2120.

Carpenter, A.E., Jones, T.R., Lamprecht, M.R., Clarke, C., Kang, I.H., Friman, O., Guertin, D.A., Chang, J.H., Lindquist, R.A., Moffat, J., *et al.* (2006). CellProfiler: image analysis software for identifying and quantifying cell phenotypes. Genome Biol *7*, R100.

Consortium, E.P. (2012). An integrated encyclopedia of DNA elements in the human genome. Nature *489*, 57-74.

Creyghton, M.P., Cheng, A.W., Welstead, G.G., Kooistra, T., Carey, B.W., Steine, E.J., Hanna, J., Lodato, M.A., Frampton, G.M., Sharp, P.A., *et al.* (2010). Histone H3K27ac separates active from poised enhancers and predicts developmental state. Proc Natl Acad Sci U S A *107*, 21931-21936.

Dignam, J.D., Lebovitz, R.M., and Roeder, R.G. (1983). Accurate transcription initiation by RNA polymerase II in a soluble extract from isolated mammalian nuclei. Nucleic Acids Res *11*, 1475-1489.

Dowen, J.M., Fan, Z.P., Hnisz, D., Ren, G., Abraham, B.J., Zhang, L.N., Weintraub, A.S., Schuijers, J., Lee, T.I., Zhao, K., *et al.* (2014). Control of cell identity genes occurs in insulated neighborhoods in mammalian chromosomes. Cell *159*, 374-387.

Hnisz, D., Weintraub, A.S., Day, D.S., Valton, A.L., Bak, R.O., Li, C.H., Goldmann, J., Lajoie, B.R., Fan, Z.P., Sigova, A.A., *et al.* (2016). Activation of proto-oncogenes by disruption of chromosome neighborhoods. Science *351*, 1454-1458.

Kagey, M.H., Newman, J.J., Bilodeau, S., Zhan, Y., Orlando, D.A., van Berkum, N.L., Ebmeier, C.C., Goossens, J., Rahl, P.B., Levine, S.S., *et al.* (2010). Mediator and cohesin connect gene expression and chromatin architecture. Nature *467*, 430-435.

Kamentsky, L., Jones, T.R., Fraser, A., Bray, M.A., Logan, D.J., Madden, K.L., Ljosa, V., Rueden, C., Eliceiri, K.W., and Carpenter, A.E. (2011). Improved structure, function and compatibility for CellProfiler: modular high-throughput image analysis software. Bioinformatics *27*, 1179-1180.

Langmead, B., Trapnell, C., Pop, M., and Salzberg, S.L. (2009). Ultrafast and memory-efficient alignment of short DNA sequences to the human genome. Genome Biol *10*, R25.

Love, M.I., Huber, W., and Anders, S. (2014). Moderated estimation of fold change and dispersion for RNA-seq data with DESeq2. Genome Biol *15*, 550.

Lubitz, S., Glaser, S., Schaft, J., Stewart, A.F., and Anastassiadis, K. (2007). Increased apoptosis and skewed differentiation in mouse embryonic stem cells lacking the histone methyltransferase Mll2. Mol Biol Cell *18*, 2356-2366.

Machanick, P., and Bailey, T.L. (2011). MEME-ChIP: motif analysis of large DNA datasets. Bioinformatics *27*, 1696-1697.

Marson, A., Levine, S.S., Cole, M.F., Frampton, G.M., Brambrink, T., Johnstone, S., Guenther, M.G., Johnston, W.K., Wernig, M., Newman, J., *et al.* (2008). Connecting microRNA genes to the core transcriptional regulatory circuitry of embryonic stem cells. Cell *134*, 521-533.

Mikkelsen, T.S., Ku, M., Jaffe, D.B., Issac, B., Lieberman, E., Giannoukos, G., Alvarez, P., Brockman, W., Kim, T.K., Koche, R.P., *et al.* (2007). Genome-wide maps of chromatin state in pluripotent and lineage-committed cells. Nature *448*, 553-560.

Okabe, S., Forsberg-Nilsson, K., Spiro, A.C., Segal, M., and McKay, R.D. (1996). Development of neuronal precursor cells and functional postmitotic neurons from embryonic stem cells in vitro. Mech Dev *59*, 89-102.

Okada, Y., Shimazaki, T., Sobue, G., and Okano, H. (2004). Retinoic-acid-concentration-dependent acquisition of neural cell identity during in vitro differentiation of mouse embryonic stem cells. Dev Biol *275*, 124-142.

Rahl, P.B., Lin, C.Y., Seila, A.C., Flynn, R.A., McCuine, S., Burge, C.B., Sharp, P.A., and Young, R.A. (2010). c-Myc regulates transcriptional pause release. Cell *141*, 432-445.

Trapnell, C., Pachter, L., and Salzberg, S.L. (2009). TopHat: discovering splice junctions with RNA-Seq. Bioinformatics *25*, 1105-1111.

Wang, S., Sun, H., Ma, J., Zang, C., Wang, C., Wang, J., Tang, Q., Meyer, C.A., Zhang, Y., and Liu, X.S. (2013). Target analysis by integration of transcriptome and ChIP-seq data with BETA. Nat Protoc *8*, 2502-2515.

Yue, F., Cheng, Y., Breschi, A., Vierstra, J., Wu, W., Ryba, T., Sandstrom, R., Ma, Z., Davis, C., Pope, B.D., *et al.* (2014). A comparative encyclopedia of DNA elements in the mouse genome. Nature *515*, 355-364.

Zhang, Y., Liu, T., Meyer, C.A., Eeckhoute, J., Johnson, D.S., Bernstein, B.E., Nusbaum, C., Myers, R.M., Brown, M., Li, W., et al. (2008). Model-based analysis of ChIP-Seq (MACS). Genome Biol 9, R137.